Winter 1975

GROWTH OF OXIDE PARTICLES IN FLAMES: A THEORETICAL AND EXPERIMENTAL STUDY OF SILICA FORMING FLAMES

NARAYANAN S. SUBRAMANIAN

GROWTH OF OXIDE PARTICLES IN FLAMES: A THEORETICAL AND EXPERIMENTAL STUDY OF SILICA FORMING FLAMES

by

NARAYANAN S. SUBRAMANIAN

B. Tech., Indian Institute of Technology (Delhi), 1968

M. S., Birla Institute of Technology and Science, 1970

A THESIS

Submitted to the University of New Hamsphire

In Partial Fulfillment of

The Requirements for the Degree of

Doctor of Philosophy

Graduate School

Engineering Ph.D. Program

Transport Phenomena

December, 1974

This thesis has been examined and approved.

Gail D. Ulrich

Thesis Director, Gail D. Ulrich, Asst. Prof. of Chem. Engg.

Stephen S T Fan

Stephen S. T. Fan, Assoc. Prof. of Chem. Engg.

John A. Wilson

John A. Wilson, Assoc. Prof. of Mech. Engg.

Harvey K. Shepard 12/26/74

Harvey K. Shepard, Associate Professor of Physics

Clarence L Grant

Clarence L. Grant, Assoc. Dir. of CIID and Prof. of Chemistry

12/20/74

Date

ACKNOWLEDGEMENT

I wish to express my deep sense of appreciation and gratitude to Dr. Gail D. Ulrich, thesis director, for his valuable guidance and inspiring discussions. His careful reading and comments on the original draft of this thesis has contributed to many improvements.

My thanks are also due to Dr. Stephen S. T. Fan, Chairman of the Department of Chemical Engineering, for his continued encouragement and financial help in the form of a teaching assistantship throughout the course of my stay as a graduate student.

The technical help rendered by Cabot Corporation, Billerica, Massachusetts, is gratefully acknowledged. M/S Hector Cochrane, F. A. Heckman, Bob Amrion, and Joe Connolly of Cabot Corporation need special mention for their encouraging discussions and invaluable advice during the course of this work. The financial support provided by the Public Service Company of New Hampshire towards this project is gratefully acknowledged.

Mrs. Brenda Cavanagh has done an outstanding job of typing which I very much appreciate.

Finally to my wife, Padma, I sincerely express my indebtedness for her constant encouragement and sacrifices over the years of my studentship.

TABLE OF CONTENTS

LIST OF TABLES

LIST OF FIGURES

ABSTRACT

GROWTH OF OXIDE PARTICLES IN FLAMES: A THEORETICAL AND EXPERIMENTAL STUDY OF SILICA FORMING FLAMES

by

Narayanan S. Subramanian

This work is a study of the growth of oxide particles in flames. Silica particles were produced through the combustion of a premixed stream of silicon tetrachloride, propane, oxygen and nitrogen. Samples were collected at various positions from 1/4 inch to 4 inches above the flame front using a specially designed nitrogen quenched vacuum probe. The collected samples, after calcination, were analyzed by nitrogen adsorptograph and the electron microscope.

The Brownian collision theory as proposed by Ulrich (1971) is modified to include the case of non-instantaneous coalescence. One serious difference is that aggregate formation is a part of the growth process and that particles exist as aggregates throughout rather than appearing only at the end of the process. Based on the modified theory, the aggregate concentration, the number of primary particles per aggregate and primary particle size have been expressed as a function of a sticking coefficient, the initial particle radius and the ratio of surface tension to viscosity. Theoretical surface area calculations are in good agreement with those measured experimentally at short and long residence times but show poor agreement at intermediate residence times. Possible sources of error are discussed in detail and suggestions for future studies are reported.

SUMMARY

Very finely divided solids are often generated in aerosol form, that is the solid is precipitated from a vapor phase. Particle formation in general occurs in numerous high temperature reaction systems. More than five million tons per year of pollutant particles are generated in the U.S. alone from coal-fired power plants (Chemical Engg. News Jan 4, 1971). Understanding of the particle formation and growth mechanism may a) lead to improved efficiencies of pollution control equipment, b) eliminate unnecessary particle production, or c) aid in quality control and product improvement in cases where fine particles find a desired end use. The investigation reported in this thesis concerns the study of particle formation and growth of silica particles.

Experimentally, silica particles were produced in a flame burning oxygen, propane, nitrogen and silicon tetrachloride. A specially designed nitrogen quench probe was used to collect particles at positions above the flame front varying from 1/4" to 4". The collected samples were then calcined, and specific surface area measurements taken using a nitrogen adsorptograph. To understand particle morphology, electron micrographs of the samples were taken. These micrographs qualitatively indicate the growth rate and quantitatively reveal the population of primary particles in the aggregates or flocs.

A particle size distribution was also obtained using a subjective technique (the Zeiss counter) to give weight percent and frequency percent distributions. These curves indicate relatively uniform particles for the each of the collected samples, with the distribution broadening as the particles grow.

The Brownian collision theory as proposed by Ulrich (1971) was modified to include non-instantaneous coalescence. In the improved model, aggregation of single particles occurs not only at the end of the growth process, but is an integral part of the collision and coalescence process which involves flocs as well as single primary particles.

A differential equation is obtained which expresses the number of primary particles per aggregate (N_p) as a function of the collision and coalescence terms

$$\frac{dN_p}{dt} = 4.84c \left(\frac{3k}{\rho}\right)^{1/2}\left(\frac{3M}{4\pi\rho A}\right) T^{1/2} C_o N_p^{0.37} R_o^{-2.5} - \frac{N_p}{R_o}\left(\frac{0.22\sigma}{\mu}\right) \qquad (19)$$

where c is a sticking coefficient, C_o is the number of silica molecules per cm^3, M is the molecular weight of silica, ρ is the density, R_o is the primary particle radius, σ is the surface tension, μ is the viscosity, A is the Avagadro number and k is Boltzmann's constant. This equation is solved numerically to obtain N_p as a function of time for various initial particle radii (R_o^o) and sticking coefficients. By comparing theoretical results with the N_p values obtained from electron micrographs, we could determine preferred values of c and R_o^o. This comparison is shown in figure 16. Specific surface areas were also predicted using the preferred values of R_o^o and c. The agreement though good at short and long residence times, is poor for intermediate values. Among the possible sources of errors, the most important is thought to be the assumption of constant sticking coefficient. Likewise use of bulk values for the viscosity and surface tension may be inaccurate for small particles. Using the experimental surface area results,

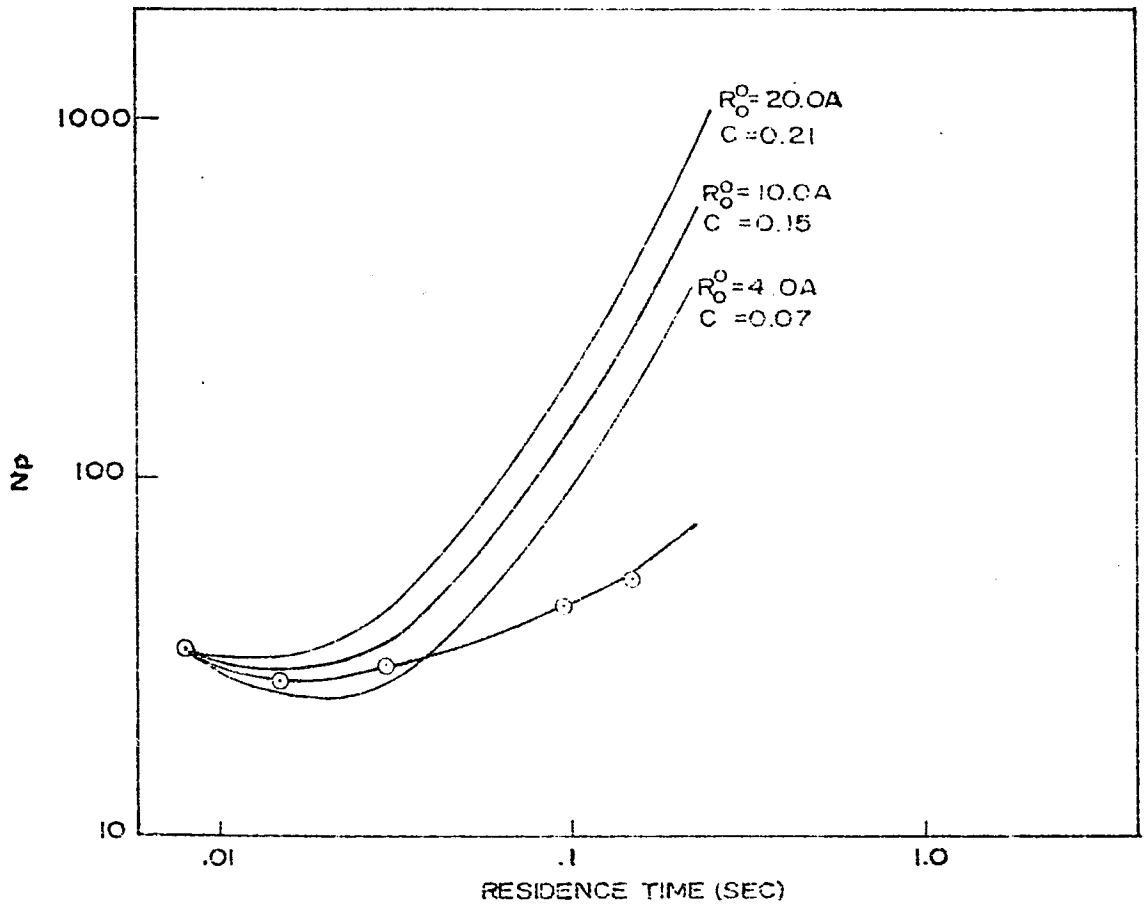

FIGURE 16. PLOT OF THEORETICAL & EXPERIMENTAL VALUES OF Np WITH RESIDENCE TIMES

hypothetical (σ/μ) values were obtained. Using these values, a modified theoretical curve was obtained which is in better agreement with experimental results (see figure 20).

Since such variables as N_p and SA are functions of R_o^o, c and (σ/μ) ratio, it is suggested that future work be concerned with systems of other oxides as well as mixtures of oxides having different physical properties. Also, more isothermal flames with broader residence time ranges would provide a better test of the theory.

It is believed that this fundamental work will aid in understanding growth phenomena in many commerical systems.

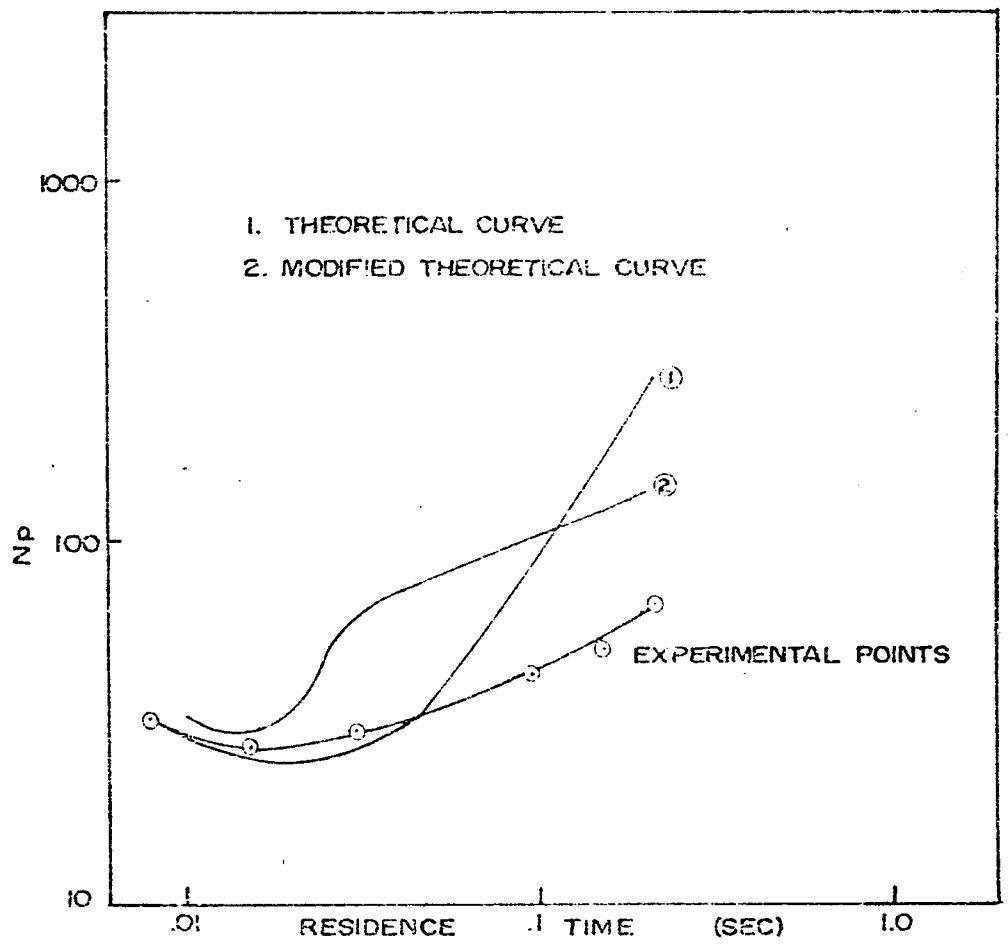

FIGURE 20. PLOT OF Np VS. RESIDENCE TIME USING THE REVISED (σ/μ) VALUES

CHAPTER I

INTRODUCTION

Particle formation at high temperatures occurs in numerous modern processes common to our industrial society. The properties of these very finely-divided solids are often far different from those of the bulk material. They are most often generated as a suspension in gases, and in many cases, their diameter has a greater effect on the properties of the system than does the chemical nature of the powder. In some instances, such a pigment manufacture and flame or plasma synthesis operations, the particle formation is intentional. In many other cases, particles are undesired by-products and when exhausted to the atmosphere, cause air pollution. Such effluents may cause serious harm to the respiratory system as well as changes in weather conditions. In any event, a basic understanding of the particle synthesis process is a necessary tool to prevent particle formation in some cases (progress in this direction has been reported for carbon produced in jet engines, Fenimore et al (1969)), collect particles when formed, or influence particle growth to controlled dimensions and texture.

Sub-micron particulate products find many commerical uses (see Table 1). Sub-micron particles emitted to the atmosphere, due to their pervasiveness, light scattering characteristics and other properties influence public health much more than larger masses of coarser dusts or smokes. Recent developments in the world energy situation leading to increased use of coal will possibly result in larger concentration of fly-ash particles in the atmosphere. A recent review by Friedlander (1973) suggests that current progress in removing more of the particulate

mass from the atmosphere may be deceptive since there is an increasing number of particles in the sub-micron range.

In processes concerned with the end use of fine particles, it is often an "aggregate" or floc which is the important unit rather than the individual particle itself. In the carbon black industry, "structure" is one of the most important parameters in the performance of a specific grade. The term "structure" was introduced to distinguish between blacks which, though similar in particle size and other parameters (surface area, surface chemistry and microstructure) differed in properties which they imparted to rubber and other systems, Medalia (1969). Other factors being equal, high "structure" blacks are more reinforcing than low "structure" blacks. It is believed that "structure" is related to the size and shape of the aggregates of carbon black. The value of the number of particles per aggregate (N_p) is thought to be the main factor affecting "structure". Figure 1 illustrates the types of aggregates found in a reinforcing grade of furnace black. The largest dimension of the aggregates varied from 440 to 5300 A° and the primary particle sizes within the aggregates are from 100 to 480 A°, Boonstra (1974).

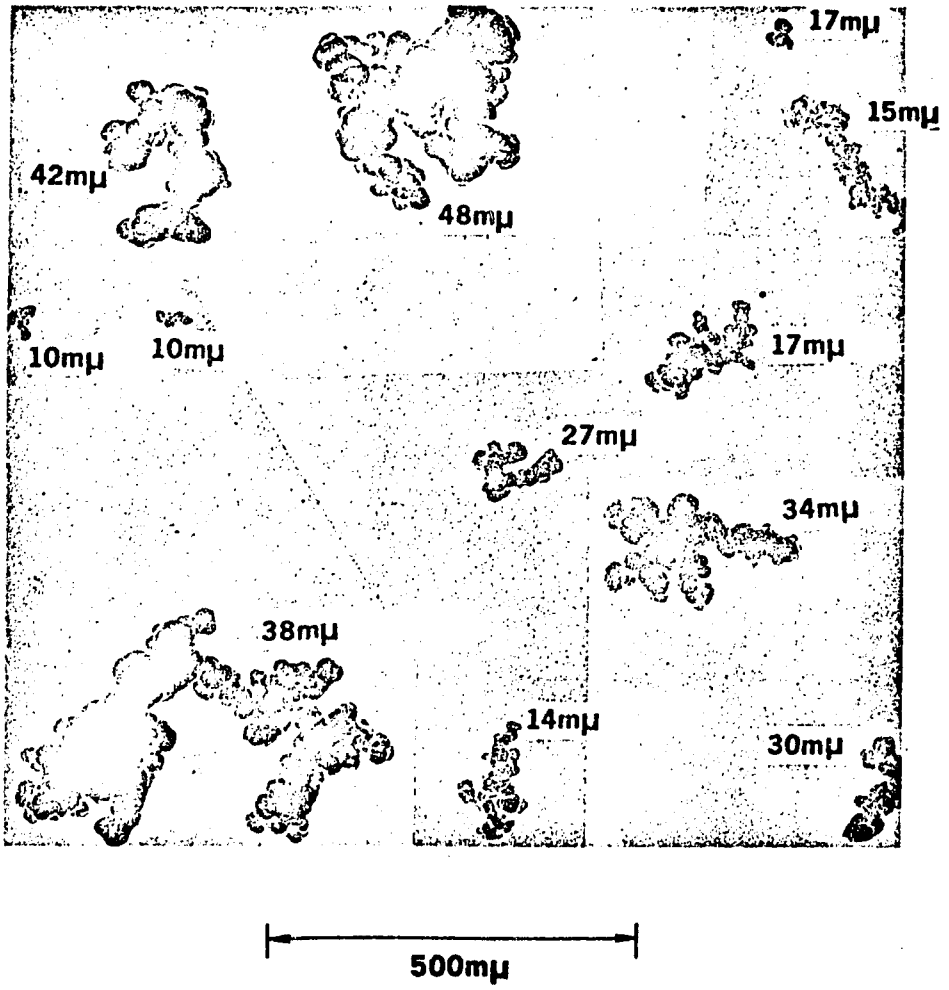

FIGURE I. MONTAGE OF AGGREGATES IN A SINGLE FIELD OF N220 CARBON BLACK

Table I (Cochrane, 1974)

Uses of Fine Particles

Particle Type	Uses
Titanium dioxide	Pigments
Carbon black	Pigments, reinforcing fillers for rubber adhesives, sealants, coatings, adsorbents
Pyrogenic silica	Liquid viscosity control agents, free flow agents, flatting agents, reinforcing fillers, sealants, coatings
Precipitated silica	Frictionizing agents, reinforcing fillers, sealants, coatings
Arc silicas	Flatting agents
Precipitated mixed oxides	Molecular sieves, catalysts
Pyrogenic alumina	Frictionizing agents
Iron oxide	Pigments

To improve the quality of very fine particles and aggregates in a given end use or to intelligently control air pollution requires an understanding of the basic formation and growth mechanism. The aim of this research investigation was to examine experimentally and theoretically the growth and aggregate formation mechanisms of silica particles. These particles were produced in a flame burning a mixture of silicon tetrachloride, oxygen, nitrogen and propane.

CHAPTER II

BACKGROUND AND SURVEY OF LITERATURE

Fundamental Growth Mechanisms:

Many earlier studies of flame particle formation have been concerned with the mechanisms of nucleation and surface reaction as the controlling steps in the ultimate particle size, Courtney (1967), Hermsen and Dunlap (1969). Amelin (1967) in his investigation on the mechanism of carbon black and aerosol formation, has explained the mechanism of formation of flame particles from the viewpoint of homogeneous vapor condensation. Stated differently, he has treated all particle formation as a nucleation problem and disregards collision coalescence completely. In his analysis Ulrich (1971) shows that nucleation in the case of SiO_2 formation from silicon tetrachloride is a necessary step in the chemical reaction process and that it has no residual effect on the growth of particles. Growth through Brownian collision and coalescence rapidly approaches a universal rate regardless of the number of initial nuclei present.

Brownian coagulation phenomena fall within two broad categories depending upon the Knudsen number (ratio of mean free path to particle diameter). In the free-molecule aerosol regime where the Knudsen number is greater than 10, kinetic theory accurately describes the collision frequency. When the Knudsen number is less than 1, in the continuum regime, the classical expression of Smoluchowski (1917) may be used. However, Wersborg, et al, (1973) have used the Smoluchowski expression for the free-molecule aerosol regime with the coagulation rate constant given by kinetic theory. Using the expression for collision frequency given by kinetic theory, Ulrich derived an expression

relating particle concentration and residence time in the free-molecule aerosol regime.

$$N = N_o \left(1 + 6.8 \times 10^{-12} N_o^{5/6} c T^{1/2} Co^{1/6} t\right)^{-6/5} \quad (1)$$

Where N, N_o are the particle concentrations, Co is the number of silica molecules present per cm^3 and c is the sticking coefficient. At large values of t, the above equation for growth rate assumes a universal expression because of rapid growth of fine particles. In terms of the more easily measured specific surface area, the theoretical expression becomes

$$SA = 1.81 \times 10^8 \left(T^{1/2} c Co t\right)^{-2/5} \quad (2)$$

This theory assumes that coalescence occurs instantaneously.

A more realistic model would allow for a finite coalescence time during which single particles and particle flocs continue to collide to form coalescing aggregates. This will be elaborated later.

Physical Mechanisms of Carbon Formation:

Bonne, Homann, and Wagner (1965) describe three different zones of carbon formation in low pressure flames. In the oxidation zone, polyacetylenes are produced and their concentration reaches a maximum near the end of the reaction zone where the so called "nuclei" are formed. In the yellow luminous portion of the flame behind the main reaction zone, small particles can be observed, and further downstream, the particle diameters increase while the number decreases. This is the so-called growth region. When the diameter reached a value of 150 - 200 A, they observed the total amount of carbon to remain constant and clusters were formed by single particles sticking together and retaining their identity.

The authors further imply that soot embryos due to the presence of hydrogen are probably tarry liquid droplets rather than solid particles, Ulrich (1969). Thus, surface reaction and random inter-particle collisions promote growth and coalescence until the soot becomes tempered. Though Bonne, et al, gave no quantitative expressions, their results appear to be in good agreement with a collision coalescence mechanism of growth.

Homann's review paper on soot formation in premixed hydrocarbon flames is an excellent survey of carbon formation mechanisms (1968). He discounts earlier theories of nucleation and chemical reaction noting that these were based mainly on the observation of single phenomena which were not always seen in true relation to the process as a whole.

The concept of nucleation has been applied very imprecisely to soot formation. Generally, those speaking of a "nucleus" mean nothing more than a small particle that is capable of further growth. In the growth of the soot particles in premixed flames, the nucleation process finishes relatively quickly and the growth phase lasts much longer. As indicated by Bonne, et al, the rapid decrease in the number of particles further downstream in the luminous zone can be quantitatively explained if at each collision two particles coalesce to form a larger particle. The shape of the particle remains spherical by the forces of surface tension. Finally when the addition of particles lags behind the coalescence of particles, aggregates or chainlike clusters result.

In carbon forming flames, the diameter of spherical soot particles is usually about 100 - 500 A. Carbon and hydrogen are the

predominant elements and the atomic C/H ratio increases from about 1 to approximately 8 as the material ages in the flame, Howard (1969). The limited range of sizes between 100 - 500 A can be explained by collision theory. In a constant mass system, the larger the diameter, the smaller will be the collision frequency. For particles greater than 500 A in diameter, the period between collisions is longer than the time required for particles to temper, so they no longer stick on colliding.

Ball and Howard (1971) measured the electric charge of carbon particles in a pre-mixed propane-oxygen flame. Their results confirm the conclusion of Weinberg (1969), that carbon particles in flames carry a positive charge. Also, they found that the charge particle ratios and average particle size tend to increase as the number of particles per aggregate decreases. However, the number of particles per aggregate as seen from Ball and Howard's paper seems to be much larger than that found by Medalia (1969), Sutherland (1971). This may have resulted from particles attached to the negative electrode, which became negatively charged and provided an electric field source attracting other particles. A qualitative observation of their electron micrographs seems to indicate that there are, in fact, large agglomerates, formed by the physical attachment of many aggregates.

Wersborg, et al, (1973) have examined the physical aspects of carbon formation in a flat acetylene-oxygen flame at 20 mm Hg pressure. Their study was similar to that of Bonne, et al, and similar trends were observed. They have extended their study into earlier growth stages in an attempt to observe the effects of nucleation and surface growth. The authors conclude that in the early stages of carbon formation, nucleation is fast relative to coagulation, and the rate of growth by

coagulation is considerably less than that of surface growth. This is reversed downstream of the reaction zone where coagulation rules. They state that electrostatic interaction between particles is responsible for the formation of particle clusters in chains instead of more compact shapes. The results and conclusions of Wersborg, et al, can be questioned for the very fine particle sizes due to the limited reliability of an electron microscope analysis. Their carbon balance and sample quality seem good but aggregates are counted as single particles rather than as a collection of smaller primary particles. In a more recent study, they report evidence that carbon particles collide at all stages of formation but the earliest collisions are obscured by surface growth which tends to fill in the boundaries between particles, Howard et al (1973). These boundaries or "necks" join adjacent spherical droplets or particles (see Figure 2). Actually because of a difference in collision probability, surface growth will be more predominant at the extremities rather than the boundaries between particles, Goodrich (1967). The necking phenomenon is more likely to result from fusion bonds between particles.

The experimental coagulation rate constant has been expressed by them in the form of the Smoluchowski equation given as follows:

$$\frac{dN}{dt} = \frac{-1}{2} KN^2 \tag{3}$$

where K is the coagulation rate constant given by

$$K = 16\gamma R_o^2 \left(\frac{\pi kT}{m}\right)^{1/2} \tag{4}$$

FIGURE 2. COALESCENCE OF SPHERICAL DROPLETS SHOWING "NECKING"

where the factor y called the correction factor by Howard is the same as the factor c, called the sticking coefficient by Ulrich. Values of y or c were obtained using Wersborg's data. Homann and Wagner's data as well as Bonne et al's data are also given below for comparison.

Wersborg's data	$y = c = 35$
Homann and Wagner's data	$y = c = 10$
Bonne et al	$y = c = 15$

These values of y suggest actual growth rates greater than predicted by kinetic theory. Howard was not able to explain the discrepancy though they cite some factors such as Van der Walls forces which can account for a small increase over the predicted rate. They also cite electrical effects, but in the case of like-charged particles, due to repulsion, the effect would be opposite to that observed.

One possible explanation for an observed Brownian growth rate larger than the theoretical, may be that aggregates are involved even in the earliest stages of collision and coalescence.

Particle Size Distribution

Hidy (1965) has solved numerically the expression for particle growth in the continuum regime (Knudsen numbers of 0.0 and 0.5) for the cases of an initially uniform distribution and a non-uniform distribution. Using reduced coordinates, dimensionless size distributions have been obtained for the above two cases. The dimensionless parameters are defined by

$$\psi_i = N_i N_o / N_T^2 \tag{5}$$

$$\eta_i = N_T (m_i / N_o) \tag{6}$$

If all particles were identical, the distribution would be represented by a single point $\psi = \eta = 1.0$. The discrete size spectrum approaches a self-preserving form (implicitly independent of time) after a certain dimensionless coagulation time. Ulrich has obtained a similar dimensionless size distribution for the free molecule aerosol regime using the kinetic theory expression for collision frequency. As growth persists the distribution broadens to a symmetrical bell shaped curve which is established within the first 10^{-7} seconds and persists throughout the balance of the growth period. After sufficiently long periods of time the self preserving distribution does not depend on the initial conditions, but varies with Kn(Knudsen number). From Ulrich's computer results we observe that the free molecule aerosol cloud has a similar distribution as developed by Hidy, but is somewhat narrower than those corresponding to lower Knudsen numbers. (Figure 3)

The results of Bonne, Homann and Wagner show that carbon particles are actually represented by a size distribution of the self preserving log-normal type. Wersborg et al (1973) find the particle size distribution is gaussian between 2 and 4 cm above the burner whereas the chain like clusters appearing later have a more log-normal distribution. They conclude that the Gaussian distribution in the early stages of carbon formation is probably due to the generation of small particles by nucleation which counteracts the development of the log normal distribution. However, it is not clear the extent to which surface growth and nucleation can change the distribution from that of log normal though the authors claim that the term "self preserving" still applies to their results.

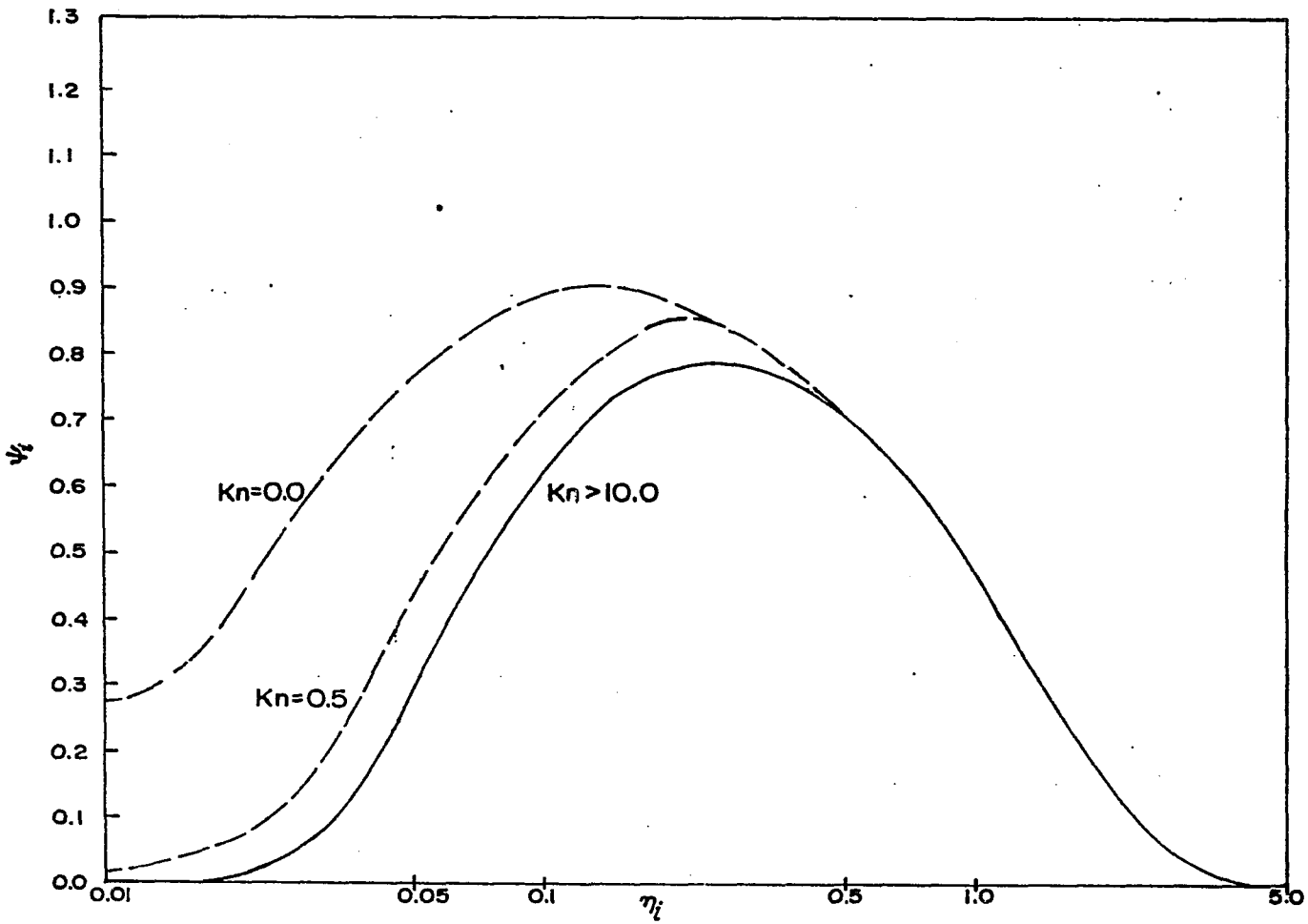

FIGURE 3. DIMENSIONLESS SIZE DISTRIBUTION ψ_i AS A FUNCTION OF THE NORMALIZED SIZE PARAMETER η_i (ULRICH, 1971)

Influence of additive ions and applied electric fields:

The application of electric fields to charged particles makes it possible to alter their trajectories. Examples of manipulating particles electrically range from established industrial practice to laboratory experiments. The electrical conductivity of a hydrocarbon flame is mainly due to chemi-ionization in the oxidation zone. Ions are formed in concentrations of about $10^9 - 10^{10}$ ions/cm^3 at atmospheric pressure, Homann (1968). Place and Weinberg (1967) studying a diffusion flame conclude that applied electric fields seem to affect all three phases in the process of carbon formation namely, nucleation, growth, and deposition. There is no doubt that a certain percentage of the soot particles in the flame are positively charged and that positive ions may act as nuclei. According to Homann the concentration of the ions in the absence of a field is several orders of magnitude lower than the concentration of hydrocarbon radicals though the author does not mention any numerical values.

Mayo and Weinberg (1970) seem to withdraw the earlier idea that ions act as nuclei in diffusion flames. Instead they suggest that carbon particles appear to pick up the same charge as the ion, namely, one charge per particle or at most two. Aggregation is suggested by them as a growth mechanism but is not treated in detail. Their results and conclusions seem to agree generally with a collision coalescence mechanism. The charge on the particle presumably reduces collision frequency. This is consistent with their observations which show a decrease in particle size with applied potential. Hardesty and Weinberg (1973) have applied this principle to particulate pollutants from flames in general. The object of their work was to attach flame ions to

particles for subsequent manipulation by applied fields. The paper does not deal with any specific mechanism , but considers suitable configurations for attachment of ions to particles. The authors have studied flame generated silica particles as well as soot. They conclude that silica particles behave very similar to carbon with regard to charge acquisition, mobility and consequent controllability by applied fields. Silica particles are also seen to be singly charged as in the case of carbon. Additive ions do not influence growth rate as long as the particle concentration is large relative to ion concentration. In our case, particle concentrations are as large as 10^{16} per cm^3 whereas maximum ion concentrations in seeded flames do not exceed 10^{13} per cm^3.

Aggregate Formation:

Electron micrographs of silica samples obtained in this experimental study show that "particles" are extensively fused together, in spite of rapid quenching. They exist as rigid, irregularly-shaped clusters or primary aggregates. The term primary "particle" has been used in the carbon black industry to mean the nodular portion of a floc which is discernible by virtue of its more or less spheroidal contour. The aggregate, then, is a collection of these primary particles. According to Ulrich, aggregation is presumed to be a concluding stage in the Brownian growth process during which particles collide and stick but due to an increase in viscosity, coalescence does not occur and primary particles retain their identity.

Medalia's (1967) theoretical work on carbon morphology shows that the shapes of carbon aggregates are consistent with those expected from a random collision mechanism. He shows that these aggregates resemble flocs synthesized by computer simulation (Figure 4).

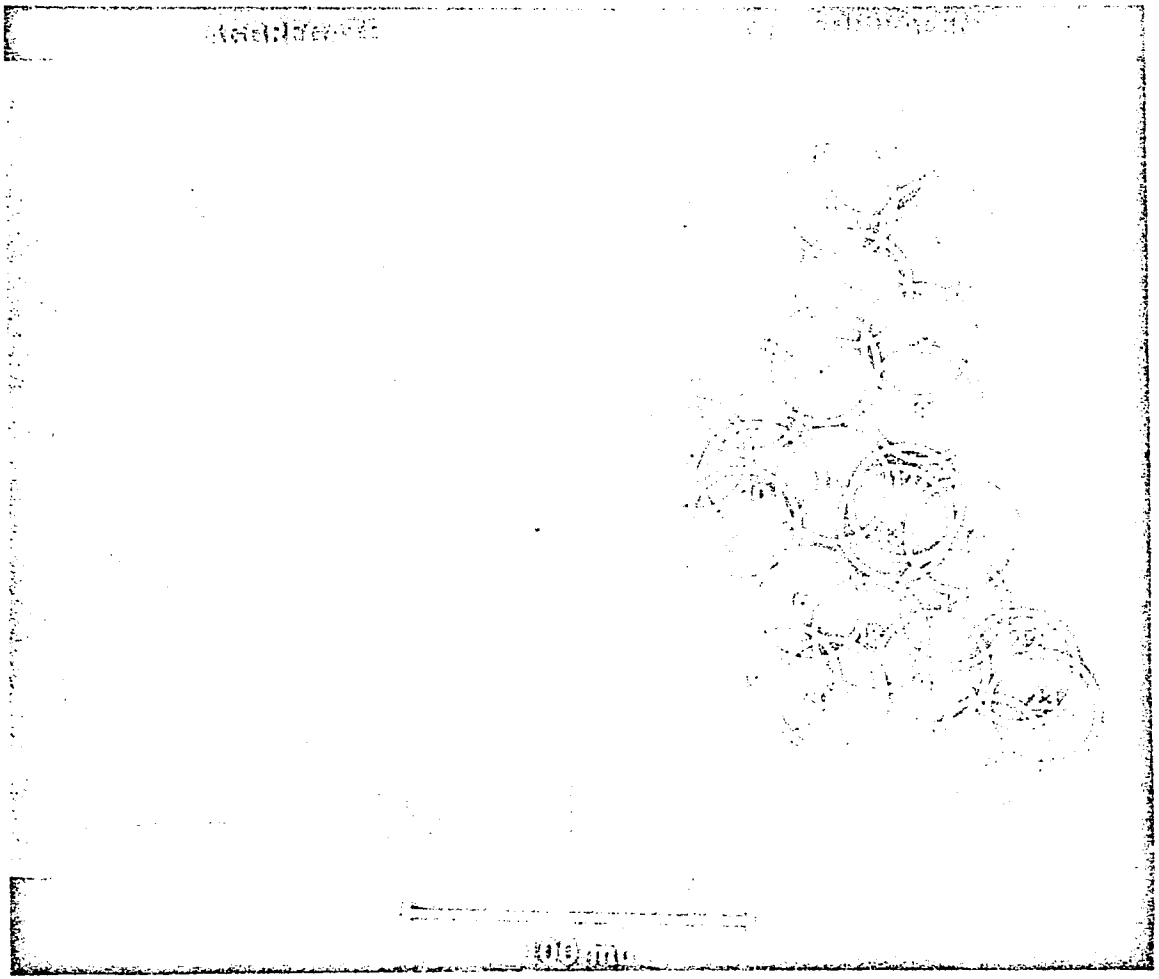

FIGURE 4. COMPARISON OF COMPUTER SIMULATED FLOCS WITH ACTUAL CARBON BLACK

(Medalia's simulation technique is not entirely rigorous since it uses a single particle addition model, whereas the true picture is probably one of collisions between primary particles and clusters as described by Sutherland (1971)). A comparison, however, of Sutherland's model with Medalia's experimental data on carbon blacks reveals that the single-particle model gives values closest to the actual while the cluster addition model predicts a structure of lower density than that observed. Sutherland reports an exponent of 1.14 for the projected area/particle number relation as compared to Medalia's experimental value of 1.15. The cluster addition model however yielded a considerably lower exponent of 1.085.

The discrepancy between Sutherland's cluster addition model and Medalia's experimental results for carbon black may simply be due to the use of an incorrect Brownian growth expression. Sutherland used an expression for collision frequency based on continuum which states that the probability of collision is independent of particle size. Based on the aggregate size observed by Medalia and Heckman (1969) the Knudsen numbers typical of some of the carbon black aggregates range between 1 and 30, indicating that much growth occurs in the free molecule aerosol regime, where the growth is very sensitive to particle size.

Howard (1969) developed a physical model for carbon formation in flames, assuming that positive ions serve as nuclei and particles are ionized during growth and aggregation. He suggested that the chain-like structure of carbon black results from interparticle electrostatic forces. As demonstrated by Medalia, charge separation is not necessary to the formation of such chain-like structures.

The theory of Brownian collision and coalescence as mentioned in this chapter is thus consistent with the interrelationships among residence time, flame geometry, concentration, "particle," and aggregate size in most high temperature particle forming systems. Qualitatively electron micrographs of silica as well as carbon blacks appear alike.

CHAPTER III

IMPROVED THEORY OF BROWNIAN GROWTH

The theory proposed by Ulrich assumes that coalescence occurs instantaneously and that growth occurs by collision of single particles. Our revised model assumes that coalescence is not instantaneous. Thus we must formulate a growth rate assuming finite fusion times and collision of aggregates or flocs as well as single particles. In this model, the aggregates are assumed to be uniform and composed of uniform primary particles.

The generalized collision frequency expression for unchanged spherical particles in the free molecule aerosol regime is given according to the relation:

$$L_{ij} = \left[8\pi kT \left(\frac{m_i + m_j}{m_i m_j}\right)\right]^{1/2} (R_i + R_j)^2 N_i N_j \qquad (7)$$

where L_{ij} = collision frequency

m_i, m_j = mass group i and mass group j

R_i, R_j = radius

N_i, N_j = concentration and k is Boltzmann's constant

For the application of eq. (7) to aggregates, the questionable parameters are the collision cross section and the mass. According to Medalia's work on carbon morphology, the floc can be represented as a sphere having an equivalent radius expressed by the following relation (1969).

$$R = (B\bar{A}/\pi)^{1/2} \qquad (8)$$

where B is a bulkiness factor and $\bar{A}$ is the projected area of the floc.

$\bar{A} = \pi R_o^2 Np^{0.87}$ where R_o is the primary particle radius and Np is the number of particles per aggregate. From a statistical count on large numbers and varieties of carbon blacks, bulkiness factor was found to be approximately 1.2. Substituting the values of B and $\bar{A}$ into the eq. (8) we have

$$R = 1.1\ R_o N_p^{0.435} \tag{9}$$

For uniform spherical particles eq. (7) reduces to

$$L_{ii} = \frac{1}{2}\left(\frac{16\pi kT}{m}\right)^{1/2} (2R)^2\ N^2 \tag{10}$$

It is assumed that the above equation can be applied to aggregates when N is the total number of aggregates per unit volume, m is the mass of the aggregate and R is the collision radius. The rate of concentration change for all aggregates can then be written as

$$\frac{dN}{dt} = -cL_{ii} = -\frac{c}{2}\left(\frac{16\pi kT}{m}\right)^{1/2} 4R^2\ N^2 \tag{11}$$

where c is the sticking coefficient (ratio of successful to actual collisions). The following expression for m applies:

$$m = N_p \frac{4}{3} \pi R_o^3 \rho \tag{12}$$

By a molecular balance, we have

$$N = \frac{3\ C_o\ M}{4\pi R_o^3 \rho A N_p} \tag{13}$$

where Co is the number of silica molecules present per cm^3, M is the molecular weight of silica and A is the Avagadro number. Elimination

of m, N, and R in eq. (11) results:

$$\frac{dN}{dt} = -4c \left(\frac{3kT}{R_o^3 \rho N_p}\right)^{1/2} (1.1\, R_o N_p^{0.435})^2 \left(\frac{3\, C_o\, M}{4\pi R_o^3 \rho A N_p}\right)^2 \tag{14}$$

Differentiating and simplyfying eq. (13), yields

$$\frac{dN}{dt} = \frac{-3\, C_o\, M}{4\pi \rho A} \left(\frac{3}{N_p R_o^4} \frac{dR_o}{dt} + \frac{1}{N_p^2 R_o^3} \frac{dN_p}{dt}\right) \tag{15}$$

To evaluate $\frac{dR_o}{dt}$ in eq. (15), consider the fusion of two equal sized spheres. The radius of the resultant single sphere is 26% greater than the initial radius. Thus for two particles

$$\frac{dR_o}{dt} \cong \frac{0.26 R_o}{t_f} \tag{16}$$

where t_f is the time for complete coalescence. t_f is given by Frenkel (1945) as

$$t_f = \frac{8\mu R_o}{\sigma} \tag{17}$$

where μ is the viscosity and σ is the surface tension. Assuming four spheres are fusing simultaneously

$$\frac{dR_o}{dt} = 0.59 \frac{R_o}{t_f} \tag{18}$$

Combination of eqs. (15) and (18) and simplification gives the following differential equation:

$$\frac{dN_p}{dt} = 4.84c \left(\frac{3k}{\rho}\right)^{1/2} \left(\frac{3M}{4\pi\rho A}\right) T^{1/2} Co\, N_p^{0.37} R_o^{-2.5}$$

$$- \frac{N_p}{R_o} \left(\frac{0.22\sigma}{\mu}\right) \qquad (19)$$

The surface tension value for silica from Kingery (1960) is 307 dynes/cm and the viscosity varies with temperature as follows (see Figure 5).

$$\mu = 1.20 \times 10^{-7}\, e^{\left(\frac{5.87 \times 10^4}{T}\right)} \qquad (20)$$

The temperature T, measured for the laboratory burner flame can be expressed as a polynomial given by:

$$T = 2.02 \times 10^3 - 4.8 \times 10^3 t - 4.0 \times 10^3 t^2 \qquad (21)$$

where t is the residence time. C_o is also a function of temperature given for the flame conditions (for silica mole fraction of 0.009) by the following expression:

$$C_o = (6.6 \times 10^{19})/T \qquad (22)$$

After substituting 2.2 g/cm^3 for ρ, 60 g/gm mole for M, 6.023×10^{23} for A, 1.38×10^{-16} erg/^{o}K for K as well as values for Co, μ, T, and σ, into eq. (19), the resulting differential equation has been numerically solved by computer simulation.

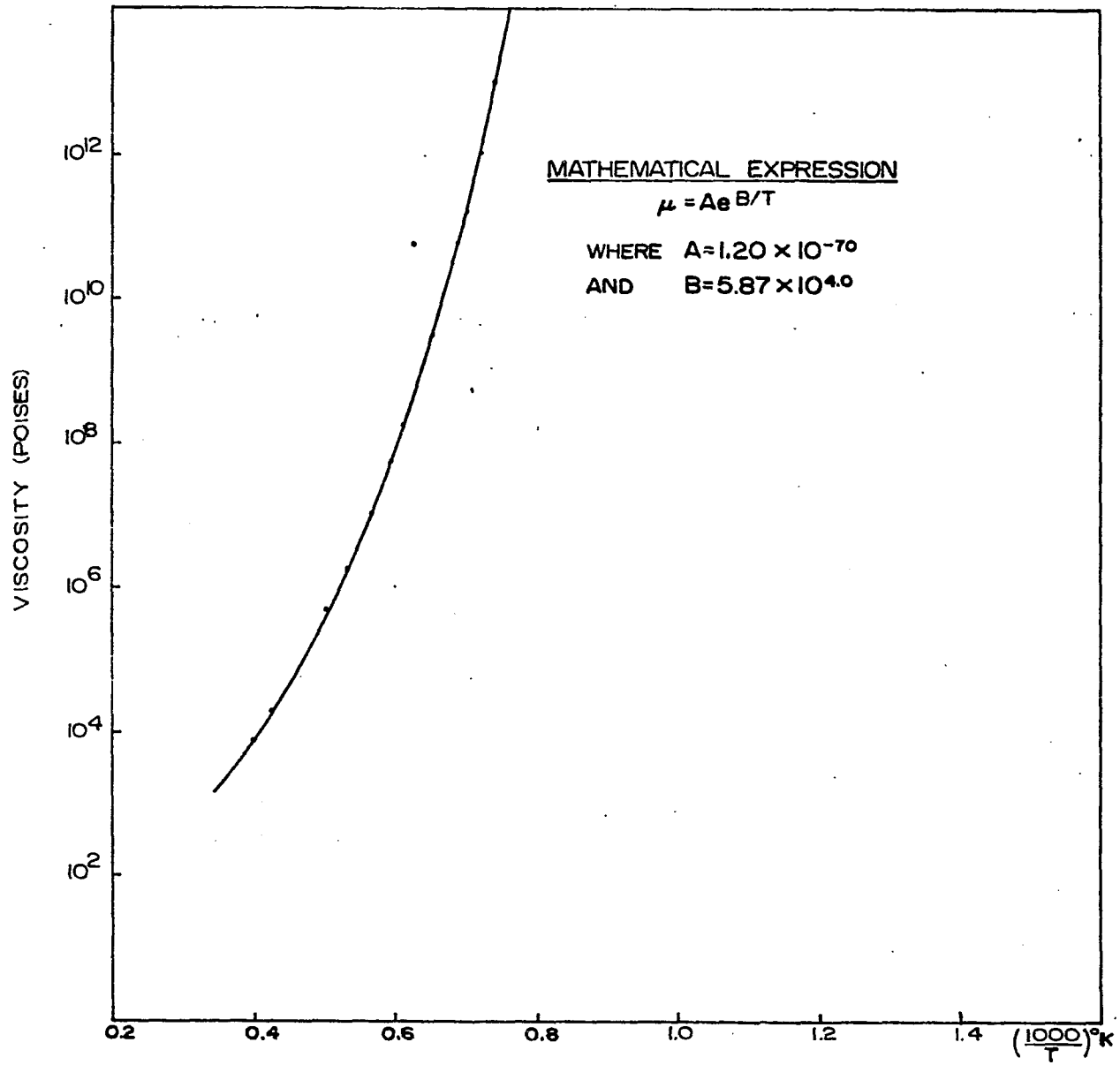

FIGURE 5. CHANGE IN LOG (μ) WITH 1/T FOR SiO_2 (KINGERY, 1960)

CHAPTER IV

EXPERIMENTAL APPROACH

Experimental Apparatus:

A detailed description of the experimental procedure and apparatus is discussed elsewhere in the companion work of Milnes (1974). In this chapter, the major components and procedure are described briefly.

A flow sheet of the experimental apparatus is shown in Figure 6. Figure 7 represents the burner arrangement. The major components of the equipment include a feed system, burner, sample probe, collection system, a gas scrubber and a steam ejector. A brief description of each of the above mentioned components is given below.

a. Feed System: The feed system includes flow meters for propane, hydrogen, oxygen, nitrogen and silicon tetrachloride. The gases are preheated to 165°F, which is above the boiling point of silicon tetrachloride, to avoid any condensation. Silicon tetrachloride is a volatile, reactive liquid. Since it reacts with atmospheric moisture to produce HCl, it must be handled with care. It is introduced by pressurizing the bottle containing $SiCl_4$ liquid and passing it through a vaporiser. The vapor is metered through a heated flowmeter. All downstream lines carrying $SiCl_4$ vapor are heated to avoid condensation.

b. Burner: The burner used in this experimental study was of the premixed, laminar, flat-flame type commonly used to study flame phenomena. (Detailed design calculations are included in Appendix A.) The burner consists of two concentric stainless steel tubes. The inside diameter is 1.5 inches (Figure 7). To achieve a uniform flow

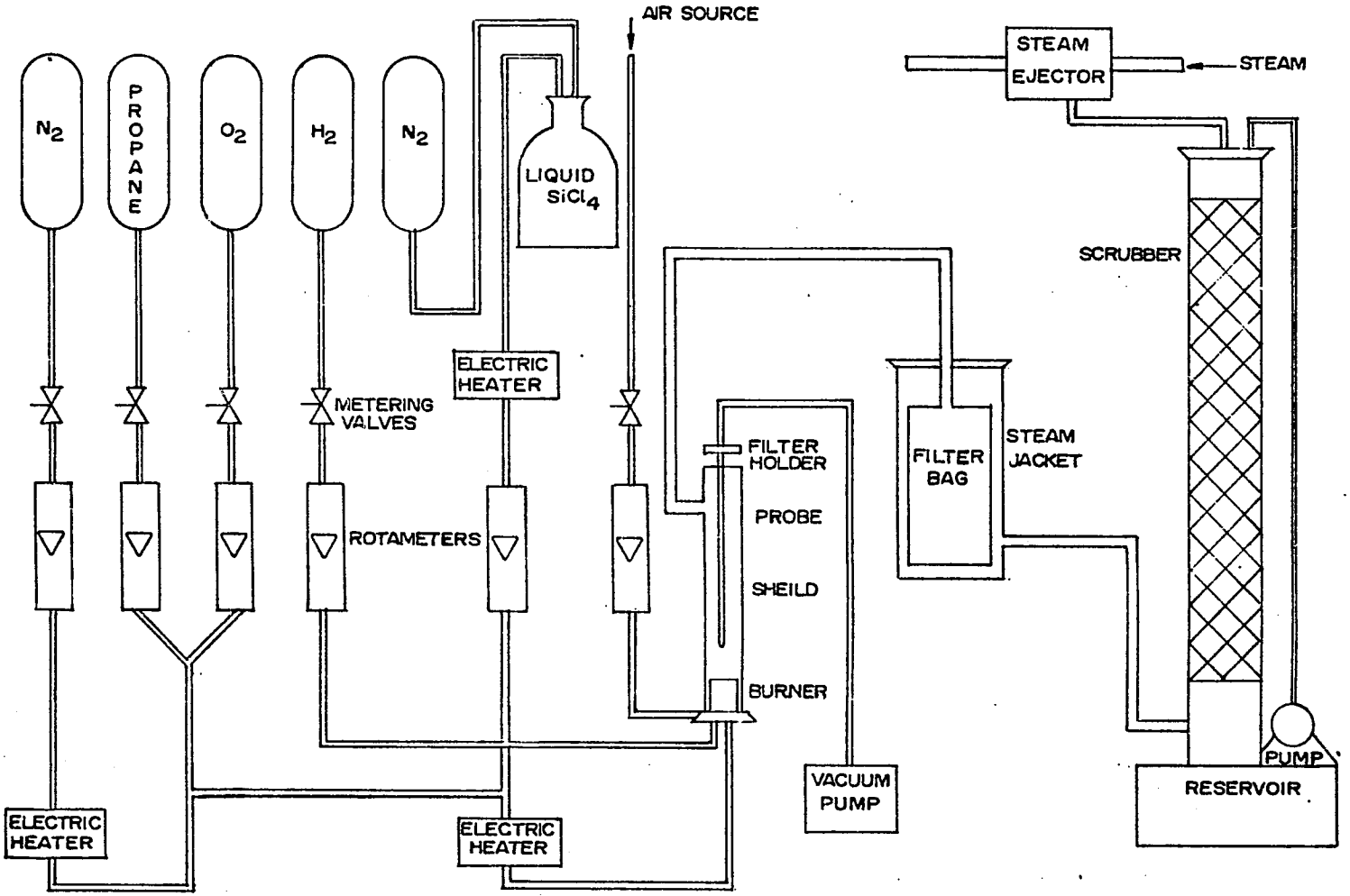

FIGURE 6. SCHEMATIC SKETCH OF THE LABORATORY COMBUSTION APPARATUS

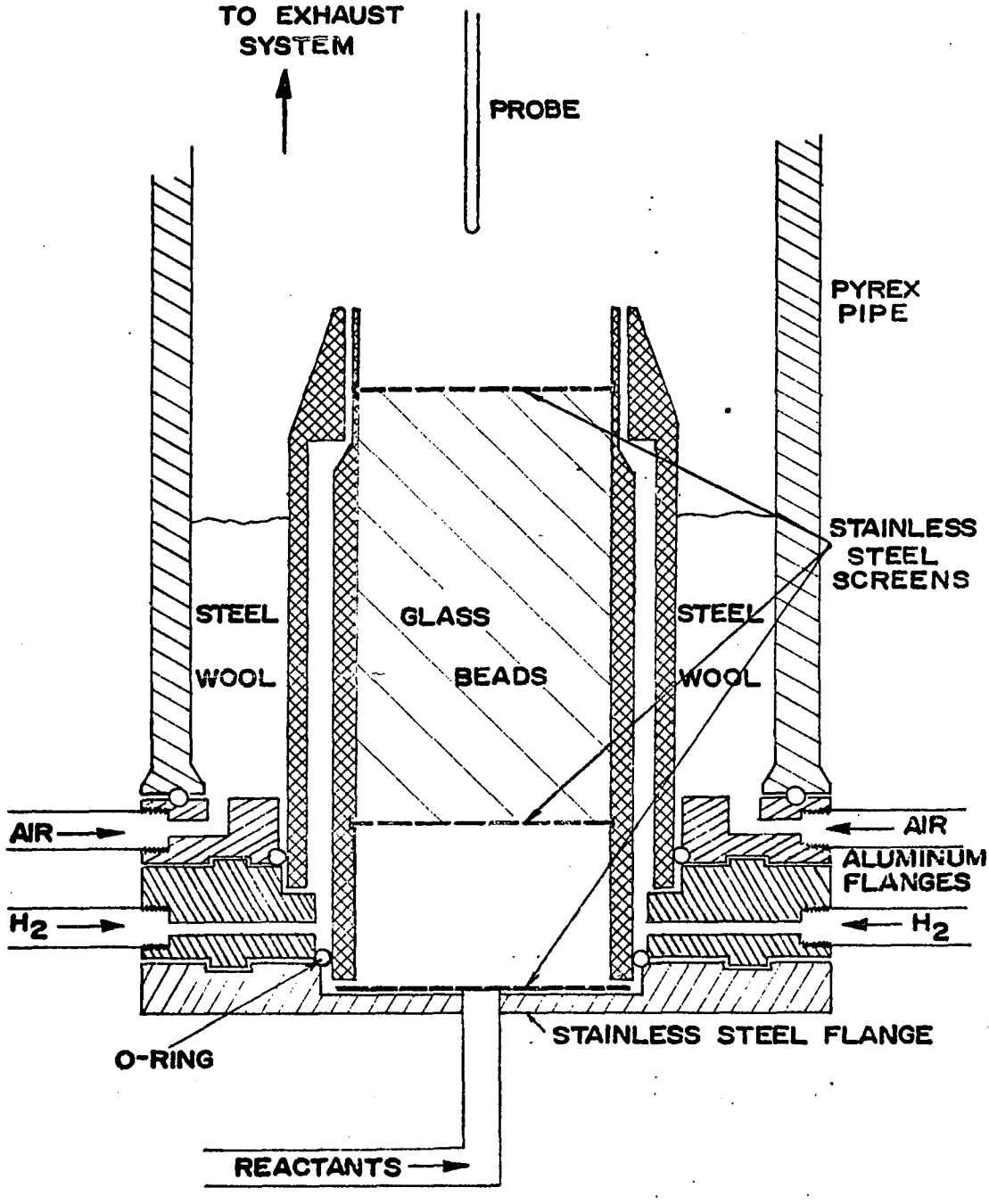

FIGURE 7. SCHEMATIC SKETCH OF THE BURNER

velocity, the inner burner was filled with 3mm dia. pyrex glass beads contained between 70 - 80 mesh stainless steel screens. This provided the required pressure drop giving a flat velocity profile to the gases as they entered the reaction zone. In principle, a flat flame can be maintained with a uniform approach stream velocity equal to the flame velocity. In practice, however, this is not possible because the flame distorts the inlet flow resulting in a button-shaped flame. By carefully adjusting the temperature and flow rates of the inlet gases, a reasonably flat flame can be maintained preventing the "button" effect. Since silica particles deposit on surfaces near the combustion zone, the flame must burn neither on the support screen nor on the tip of the burner, otherwise the screen becomes fouled or deposition of silica around the burner edge causes flame instability. To anchor the flame away from the metal surface, hydrogen was passed through a small, annular mantle ring (.005" thick). The burner was operated at atmospheric pressure. A pyrex chamber and air curtain were used to shield the flame from ambient disturbances and to minimise mixing of the combustion products.

c. Sampling Probe: The probe used to withdraw samples from the flame was fabricated from two concentric stainless steel tubes of 5/32" OD respectively (see Figure 8). A quartz probe similar to that employed by Fristrom and Westenberg (1965) became plugged rapidly with silica particles. A detailed description of the stainless steel probe used in our system is included in Appendix B. The critical diameter, that of the sampling hole was 0.020 inches. Initially, before collecting a sample, nitrogen was introduced through the annulus and forced through the tip to prevent clogging. To begin sampling,

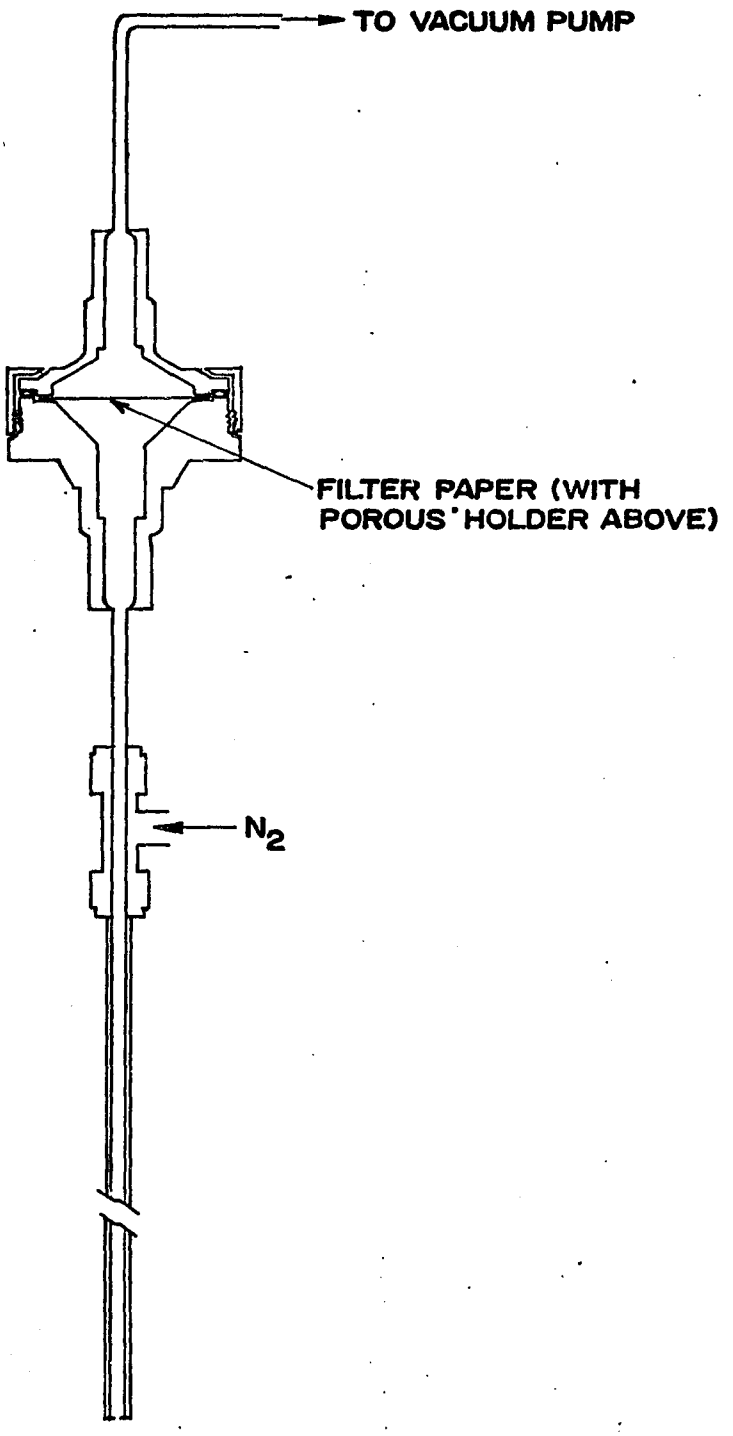

FIGURE 8 . SCHEMATIC SKETCH OF SAMPLING PROBE

the vacuum pump was switched on and the nitrogen served to quench the sample and convey silica particles to the filter holder. The filter holder used to collect particles was of the Gelman type and glass fiber filters 47mm in diameter (Pore size = .9μ) were used. The filter holder was heated to a temperature of 200°C to avoid condensation of HCl and water. Samples were collected for a period of 10 - 30 minutes and were weighed to check the material balance. They were steam calcined to remove adsorbed HCl and specific surface areas were measured. Samples were collected both from center-line and off-center positions to check the radial uniformity of the flame.

Bulk filtration of silica particles from the exhaust gas stream was accomplished using a bag filter with teflon felt bags. The filter was contained in a steam-jacketed vessel to prevent condensation of hydrochloric acid.

The gas scrubber was employed to absorb HCl from the exhaust gas before venting. It consisted of a pyrex tower 6 inches in diameter packed with Intalox saddles and irrigated with a solution of sodium hydroxide.

A standard steam ejector was used to withdraw the exhaust gases.

Experimental Procedure and Analysis:

The experimental procedure was as follows: Initially, a hydrogen mantle flame was ignited. Then a propane, oxygen, nitrogen flame was established in the burner. After allowing approximately 30 minutes for steady state in the vaporiser, silicon tetrachloride was introduced into the propane flame. The probe was positioned above the flame front and the vacuum pump was switched on for a period of ten to

thirty minutes to collect the sample. Each sample was then weighed and labelled.

Normally, silica samples as collected contain significant quantities of adsorbed HCl. To remove this, the samples were calcined in a steam-air atmosphere at 700°F for about 60 minutes. Specific surface areas were then measured using a nitrogen adsorptograph. Preparation of samples for electron microscope anlaysis is described in detail in Appendix C. Briefly, 3mg of the sample was weighed into a vial to which 30cc of diluted collodion (diluted 1:40 using ethyl acetate) was added. Using ultrasonic energy, the sample was dispersed and a clean glass slide was dipped into the dispersed solution, drained of excess liquid and dried in air. After about 30 minutes, the edges of the film were scored, floated off in distilled water and picked up on a carbon substrate grid (300 mesh). After soaking overnight in ethyl acetate, the grids were ready for the electron microscope. Prior to employing the dispersion procedure, samples were collected directly on a carbon grid and electron micrographs were taken. Some of these have been included in Appendix C. Because of overlapping of particles and aggregates, they clearly are not suitable for quantitative analysis. The above mentioned procedure was developed by Medalia and Heckman (1969) for carbon black, and was refined for these silica samples after considerable trial and error.

Electron micrographs of the samples were obtained using the UNH Philips Electron microscope EM-200, at a final magnification of 100,000X. To increase objectivity, photographs were taken of pre-selected random fields. Using the Zeiss counter, particle size distributions of the samples were obtained, from the 8 x 10 prints. To

represent the samples in a statistically reliable manner, the number of measurements on the Zeiss counter was chosen to be at least 1000 particles.

CHAPTER V

RESULTS

Numerous samples were withdrawn at distances ranging from 1/4" to 4" away from the flame front and at two silicon tetrachloride concentrations. The flame front was not visibly disturbed when the probe was 1/4" or further away from the flame front.

Specific surface areas were measured for each sample. Residence times ranged from 10 to 200 milliseconds and surface areas varied from 400 to 151 m^2/g. Specific surface area results and residence times are shown in Table II. Since the temperature varies along the axis of the flame front, residence times have been corrected accordingly. The theoretical flame temperature for our laboratory flame was obtained using the computer program for the evaluation of equilibrium temperature and compositions of complex chemical systems developed by Cruise (1964) (see Appendix D).

Samples were also analyzed with the electron microscope to provide information about particle morphology and size distribution. All of the samples were in the form of aggregates of fairly monodisperse rounded particles. They appear to be fused rather than loose clusters. Electron micrographs of some of the collected samples are shown in figures 9 through 12. These samples were obtained at a silicon tetrachloride concentration of 0.009. Their specific surface areas are 358, 349, 203 and 151 m^2/g corresponding to residence times of .008, .013, 0.095, and .210 seconds respectively.

Particle size distributions of these samples were evaluated using a Zeiss counter. It is a semi-automatic instrument for transmitted

TABLE II

Experimental Specific Surface Area and Residence Times

Height above flame front, inch	Residence time for constant temperature of 1975°K seconds	Residence time for temperature distribution using theoretical flame temperature (seconds)	Residence time for temperature distribution from theoretical h (secs)	Specific Surface Area M^2/gm
		Silica mole fraction = 0.009		
0.25	.008	.008	—	358.0
0.375	.013	.013	—	349.0
0.50	.017	.017	.024	338.0
0.625	.021	.021	.030	313.0
0.75	.026	.026	.036	306.0
0.875	.030	.030	.042	296.0
1.0	.035	.035	.048	284.5
1.25	.043	.044		276.0
1.50	.052	.053	.073	259.0
2.0	.068	.072	.099	244.0
2.5	.086	.095	.127	203.0
3.0	.103	.126	.161	191.0
4.0	.137	.210	.253	157.0
		Silica mole fraction = 0.008		
0.375	.012	.013	—	401.0
0.50	.017	.017	.024	376.0
0.625	.021	.021	.030	371.0
0.75	.026	.026	.036	329.0
0.875	.030	.030	.042	327.0
1.0	.035	.035	.048	298.0
1.5	.052	.053	.073	269.0
2.0	.068	.072	.099	261.0
2.5	.086	.095	.127	220.0
4.0	.128	.210	.253	173.0

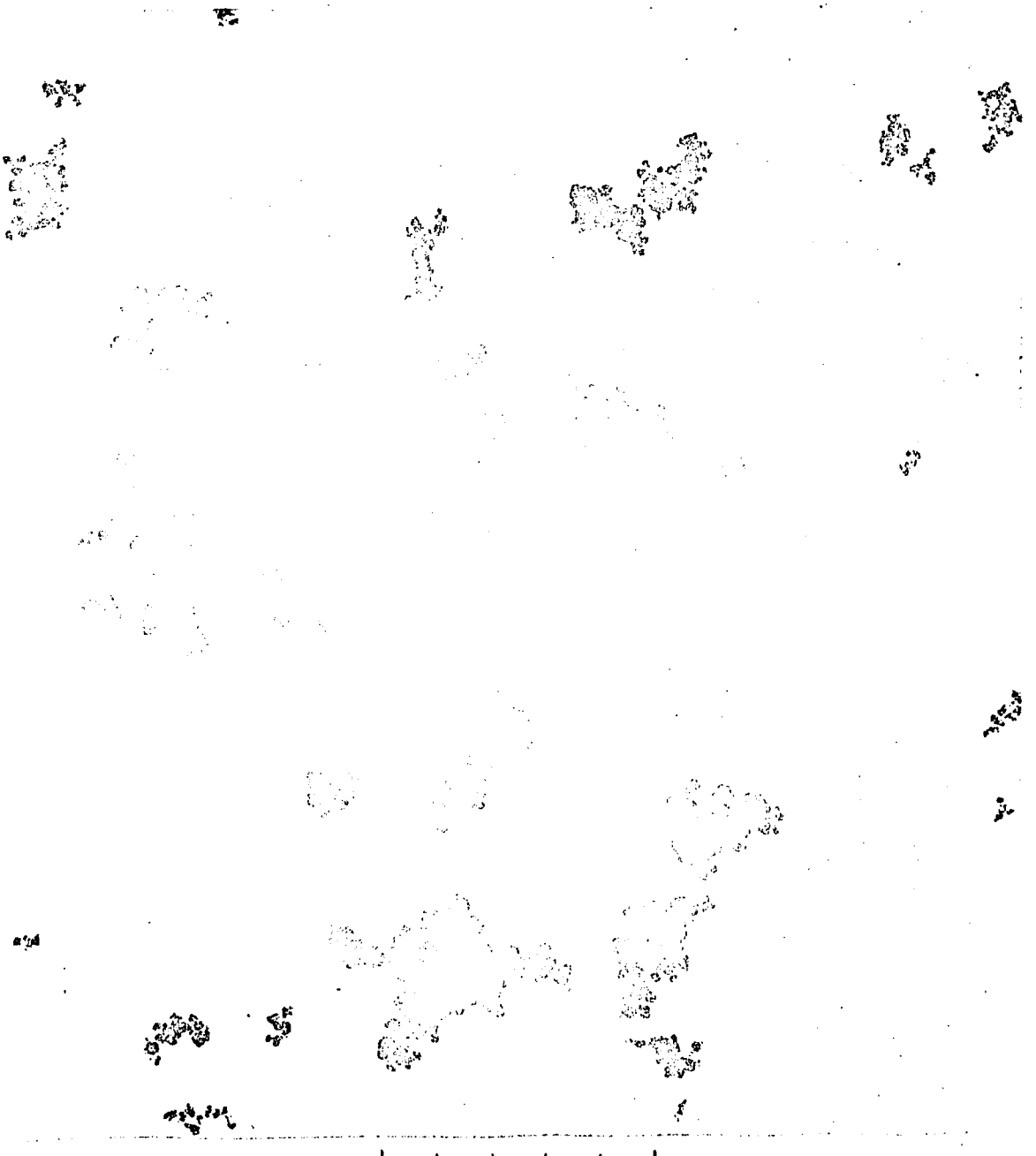

FIGURE 9. TRANSMISSION ELECTRON MICROGRAPH

SURFACE AREA = 358 M^2/G

FIGURE 10 TRANSMISSION ELECTRON MICROGRAPH

SURFACE AREA = 349 M^2/G

FIGURE 11.. TRANSMISSION ELECTRON MICROGRAPH

SURFACE AREA = 203 M^2/G

FIGURE 12. TRANSMISSION ELECTRON MICROGRAPH

SURFACE AREA = 151 M^2/G

light measurements on translucent points. This instrument is designed so that a round spot of light is projected on to the translucent point, the spot size is adjusted to match the area of a given particle and the particle diameter is recorded in one of 48 categories. In each case, at least a 1000 particles were counted to represent the samples in a statistically reliable manner. The information from the Zeiss counter was fed to the computer to obtain various particle size parameters. These parameters are defined as follows:

$$\text{Surface mean diameter DA} = \frac{\Sigma n_i d_i^3}{\Sigma n_i d_i^2}$$

$$\text{Arithmetic mean diameter DN} = \frac{\Sigma n_i d_i}{\Sigma n_i} \qquad (23)$$

$$\text{Standard arithmetic deviation} = \sqrt{\frac{\Sigma (d_i - D_N)^2}{\Sigma n_i}}$$

$$\text{Surface area by electron microscope} = \frac{6000}{\rho \times \text{DA } (m\mu)}$$

Surface mean diameter (DA) is used to calculate the specific surface area from the electron micrograph results. The above parameters have been used to arrive at particle size distributions. These are shown in figures 13 and 14. The results from the Zeiss counter analysis are tabulated (see Table III) along with N_P, the number of particles per aggregate. In each case a total of 100 aggregates was counted.

Specific surface area results determined from electron micrographs differ significantly (about 35% average) from those measured from

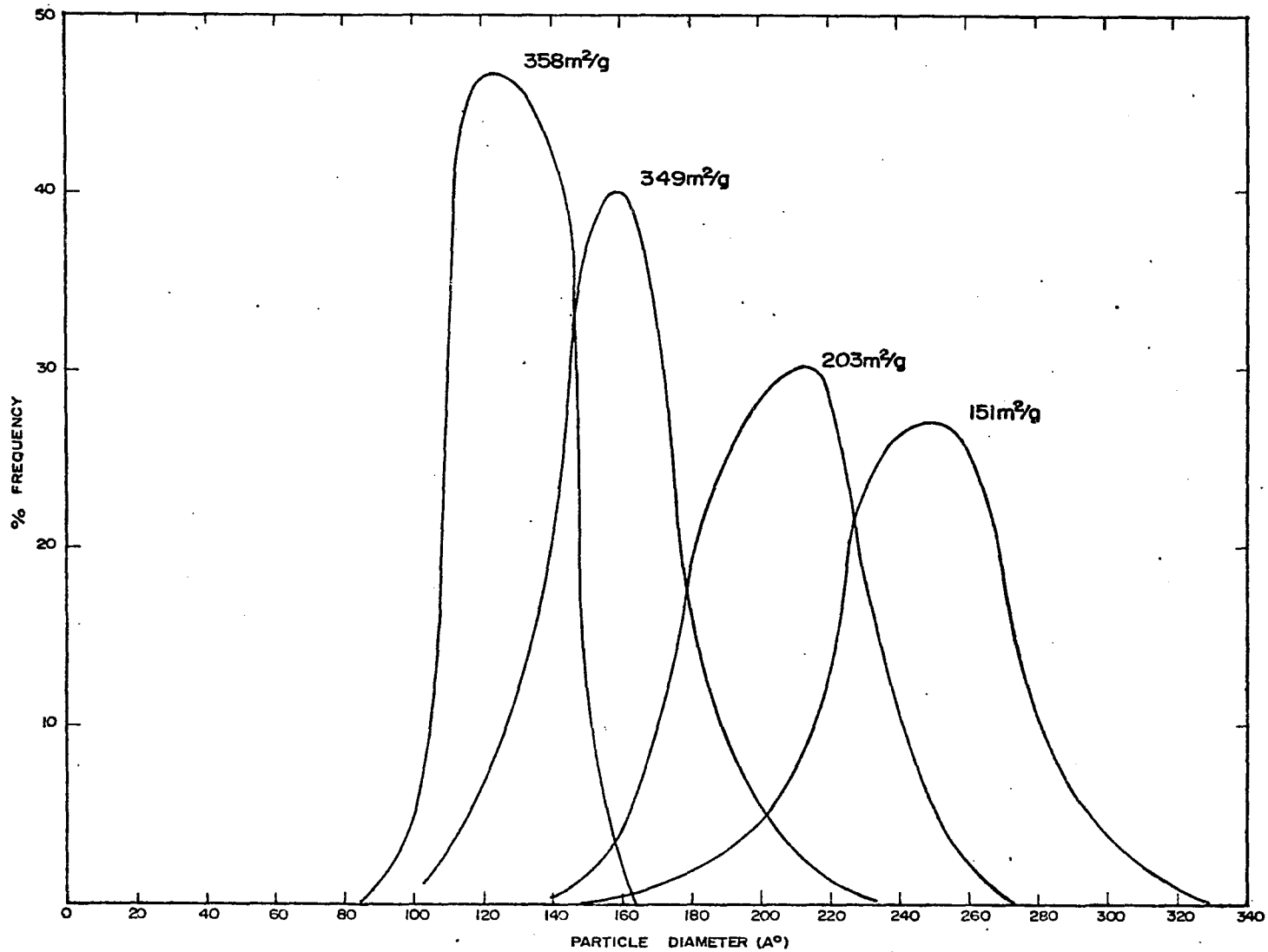

FIGURE 13. PARTICLE DIAMETER DISTRIBUTIONS WITH ADSORPTOGRAPH SURFACE AREAS

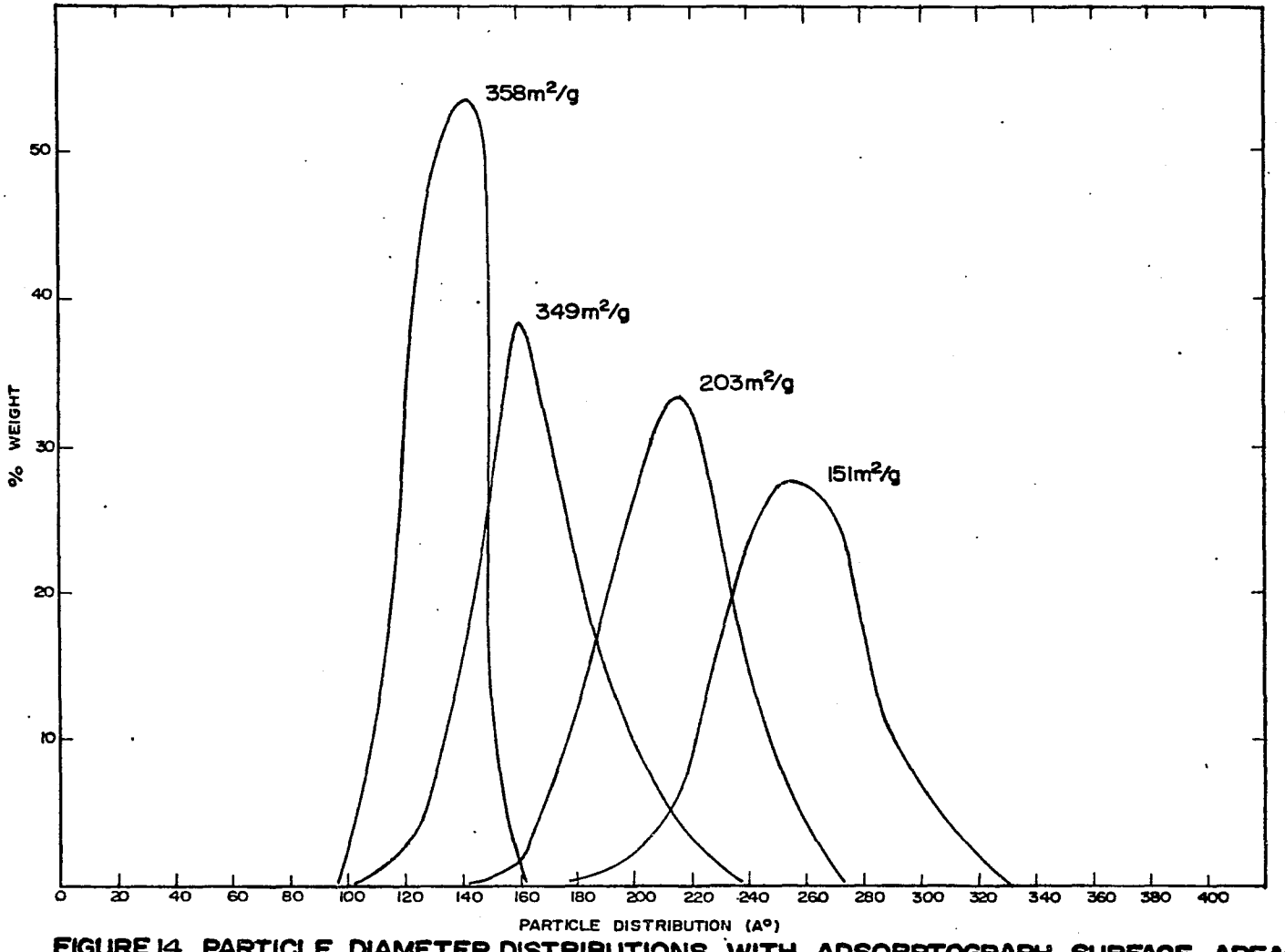

FIGURE 14. PARTICLE DIAMETER DISTRIBUTIONS WITH ADSORPTOGRAPH SURFACE AREAS

Table III

Summary of Particle Size Distribution

From Zeiss Counter Analysis

S NO	Height from the flame inch	SA from NA m^2/gm	SA from EM m^2/gm	DN (^oA)	DA ^oA	Sigma	N_P
1	0.25	358.0	207.0	129.0	131.3	1.26	33
2	0.375	349.0	165.0	159.0	164.8	2.15	27.0
3	2.5	203.0	130.0	205.2	210.1	2.27	44.0
4	4.0	151.0	108.0	248.4	252.4	2.44	77.0

the adsorptometer. This is due to the so called electron microscope contamination which results from interaction of the electron beam with organic molecules adsorbed on the bombarded specimen surface. The molecules are due to vapors which are always present in a continuously pumped demountable vacuum system arising from grease around the vacuum seals as well as from diffusion pump oil. The organic molecules which condense on surfaces which are exposed to the beam will be transformed into graphitic matter when struck by the electrons. Thus a layer of such material on the specimen can obscure the fine detail as well as alter the quantitative measurements.

CHAPTER VI

DISCUSSION OF RESULTS AND CONCLUSIONS

Particle Size Distribution

Theoretical particle size distributions were presented by Ulrich (1971) for the simple collision model. Experimental results determined from electron micrographs are shown in figures 13 and 14. Because of limited reliability of E.M. particle curves (see Appendix E) no quantitative conclusions can be stated. It will be noted only that the size distribution appears very narrow for all the samples differing only in the location of the peaks. This is qualitatively consistent with the simplified theoretical predictions. Due to the limits of E.M. techniques for size distribution analysis, further discussion of this is not presented. Earlier investigators, Wersborg (1973), Bonne, et al, (1965) have, however, used this approach. Heckman (see Appendix E) commenting on this, describes it as an "excercise in futility".

According to the previously proposed collision coalescence theory, specific surface area is a function of the sticking coefficient c. However, this model is based on instantaneous coalescence. If, on the other hand the rate of coalescence is controlling and the number of particles in a floc is large, surface area will be independent of c. That is, the fusion rate will be independent of collision rate as long as each particle is completely surrounded by other primary particles in the floc. Under these conditions the rate of change of surface area will also be independent of N_P and a function only of R_o. For the silica system having a high viscosity, coalescence does appear to control. A

theoretical rate expression which includes finite coalescence time has been developed in Chapter III. The final equation (eq. 19) predicts that the number of particles per aggregate (N_P) is a function of both collision and coalescence terms:

$$\frac{dN_P}{dt} = 4.84\, c \left(\frac{3k}{\rho}\right)^{1/2} \left(\frac{3M}{4\pi\rho A}\right) C_o N_P^{-0.37} R_o^{-2.5} - \frac{N_P}{R_o} \left(\frac{.22\sigma}{\mu}\right) \qquad (19)$$

This equation has been simulated on the IBM 360/50 and N_P obtained as a function of time for various sticking coefficients and primary particle radii. The results show that N_P in our system is increasing; indicating that aggregates are always present. Initial particle radius values of 4.0,10.0 and 20.0 A° and sticking coefficient values of 1.0, .1 and .01 were considered. (Using thermodynamic reasoning Ulrich suggests that any silica molecule bimolecular or larger is stable under our flame conditions, hence, values of initial particle radius less than 4° A were not considered.) The results of the simulation have been plotted and are shown in figure 15.

According to the simplified theory, in which instantaneous coalescence is assumed, surface area is not a function of R_o^o, the initial primary particle radius. (Note that R_o^o is defined differently from R_o which is the primary particle radius at any time.) However, when coalescence is controlling, according to the modified theory, surface area is a function of both R_o^o as well as residence time whereas N_P is a function of R_o^o and sticking coefficient c as well as residence time. Thus, there exist two arbitrary parameters, c and R_o^o. Since the data from the electron micrograph analysis for N_P are

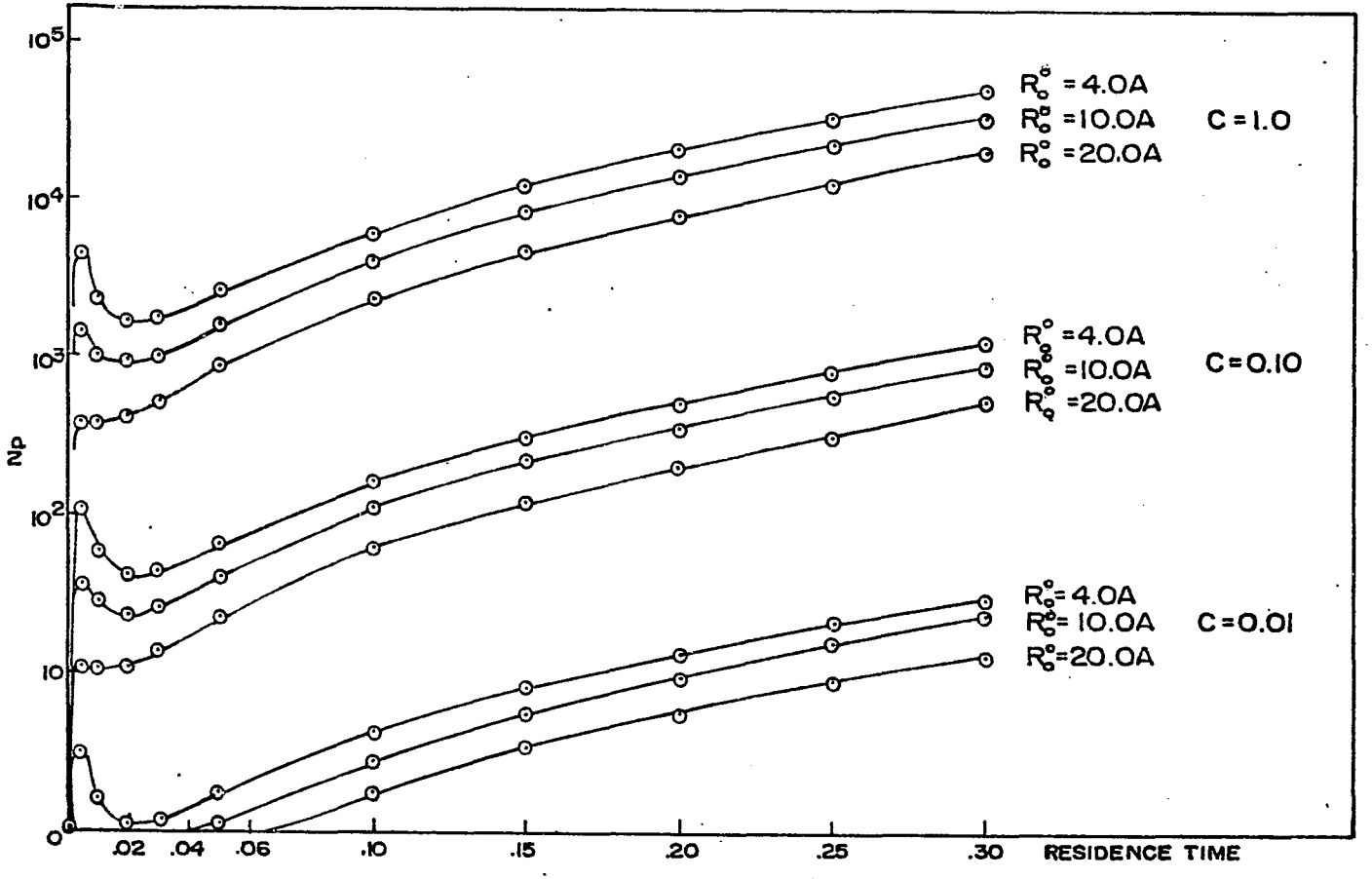

FIGURE 15. PLOT OF LOG Np VS. RESIDENCE TIME

reasonably reliable, they have been utilized to determine R_o^o and c. In all cases values were selected so that the curves passed through the first datum point, corresponding to a residence time of 8 milliseconds. Based on the results shown in figure 16, values of 0.07 for c and 4°A for R_o^o seem to provide the best fit. (Numerical values are listed in Table IV.) This approach is somewhat tenuous since the electron micrograph results are not precisely quantitative. The reasons for fitting curves to the first datum point is that N_P results are less accurate for larger aggregates, Medalia (1969). Using the value of R_o^o and c above, surface areas were calculated. These are shown in figure 17. The curve for the preferred values (c = .07 and R_o^o = 4.0A) is shown in figure 18 where experimental specific surface area data are also plotted. The agreement, though good at short and long residence times is poor for intermediate values. Possible reasons for the discrepancy are:

1. The theoretical equations are incorrect.
2. The experimental data are in error.
3. The sticking coefficient may be a function of other variables rather than constant as assumed here.
4. Use of bulk values for the viscosity and surface tension in the theoretical equations may be in error for these smaller particles.
5. Values of N_P obtained from two dimensional electron micrographs may be erroneous especially in larger aggregates.

The theoretical expression based on kinetic theory and Frenkel's (1945) coalescence expression are considered sound. The possible errors which may be introduced into the equation may be due to:

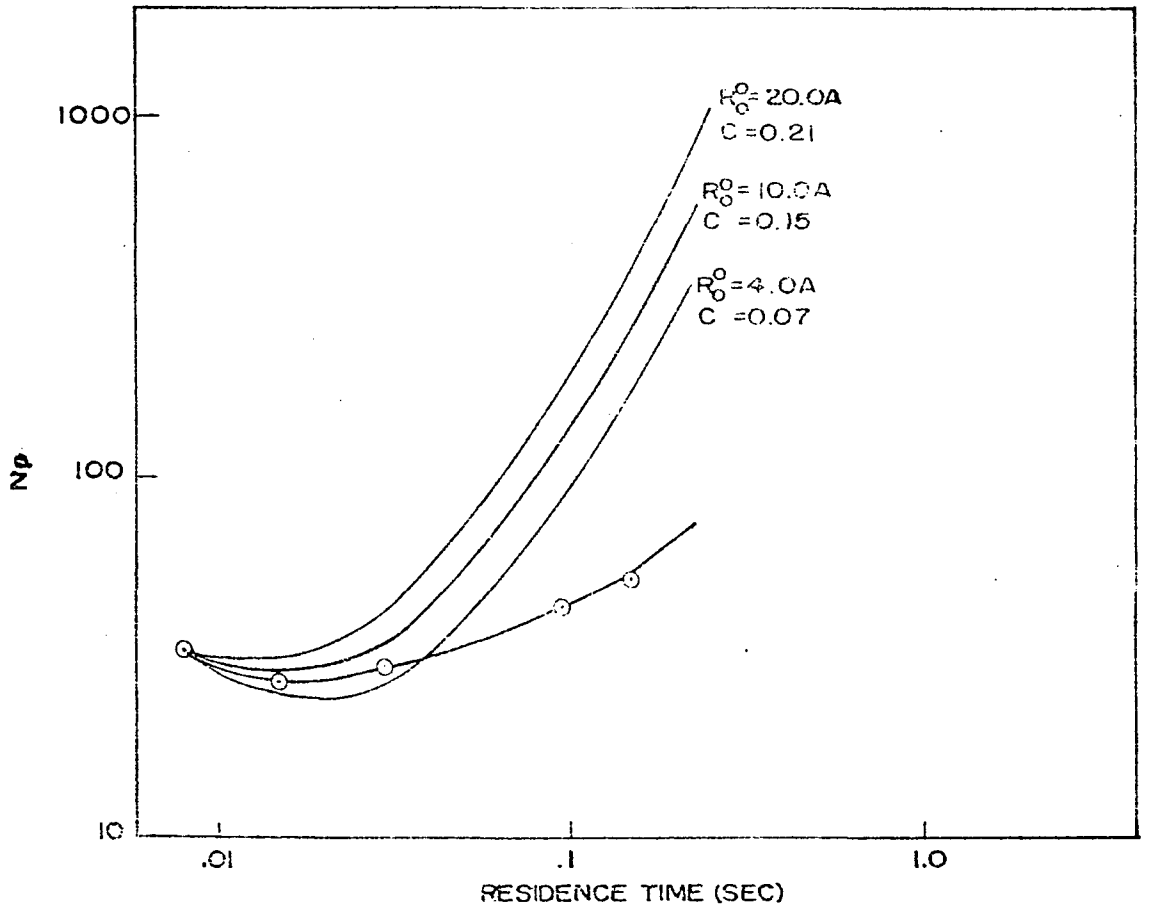

FIGURE 16. PLOT OF THEORETICAL & EXPERIMENTAL VALUES OF Np WITH RESIDENCE TIMES

Table IV

Values of N_P obtained from theoretical expression by Curve fitting through the first experimental datum point

Residence time (seconds)	c = 0.07 R_o^o = 4 A	c = .15 R_o^o = 10°A	c = 0.21 R_o =02.0A°	Experimental N_P
	N_P	N_P	N_P	
.008	33.0	33.0	34.0	33.0
.015	26.0	30.0	33.0	27.0
.02	24.0	29.0	36.0	--
.03	25.0	33.0	44.0	30.0
.05	37.0	52.0	74.0	--
.095	92.0	135.0	200.0	44.0
.15	173.0	259.0	388.0	52.0
0.21	289.0	475.0	718.0	77.0

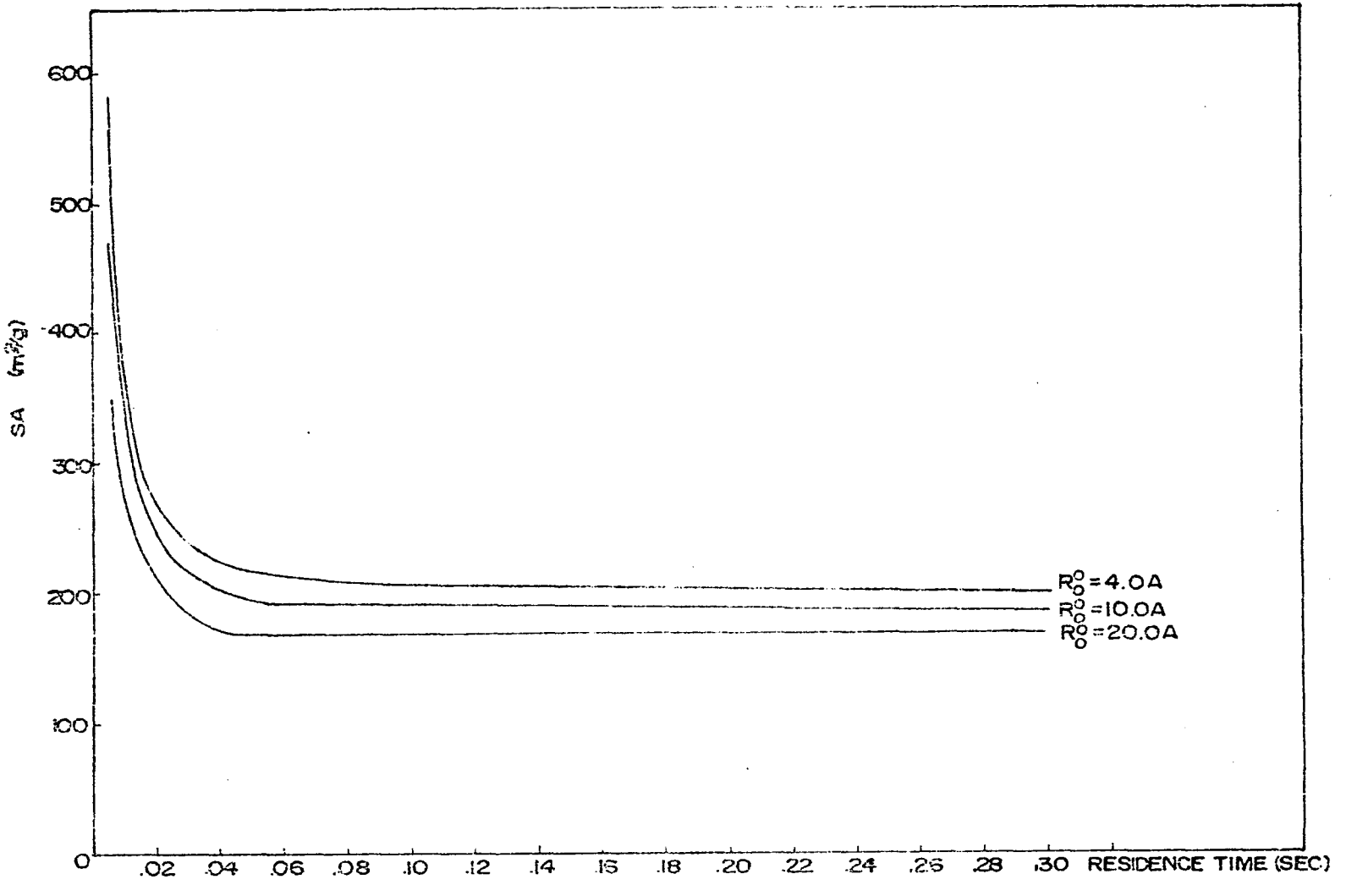

FIGURE 17. PLOT OF THEORETICAL SURFACE AREA VS. RESIDENCE TIME

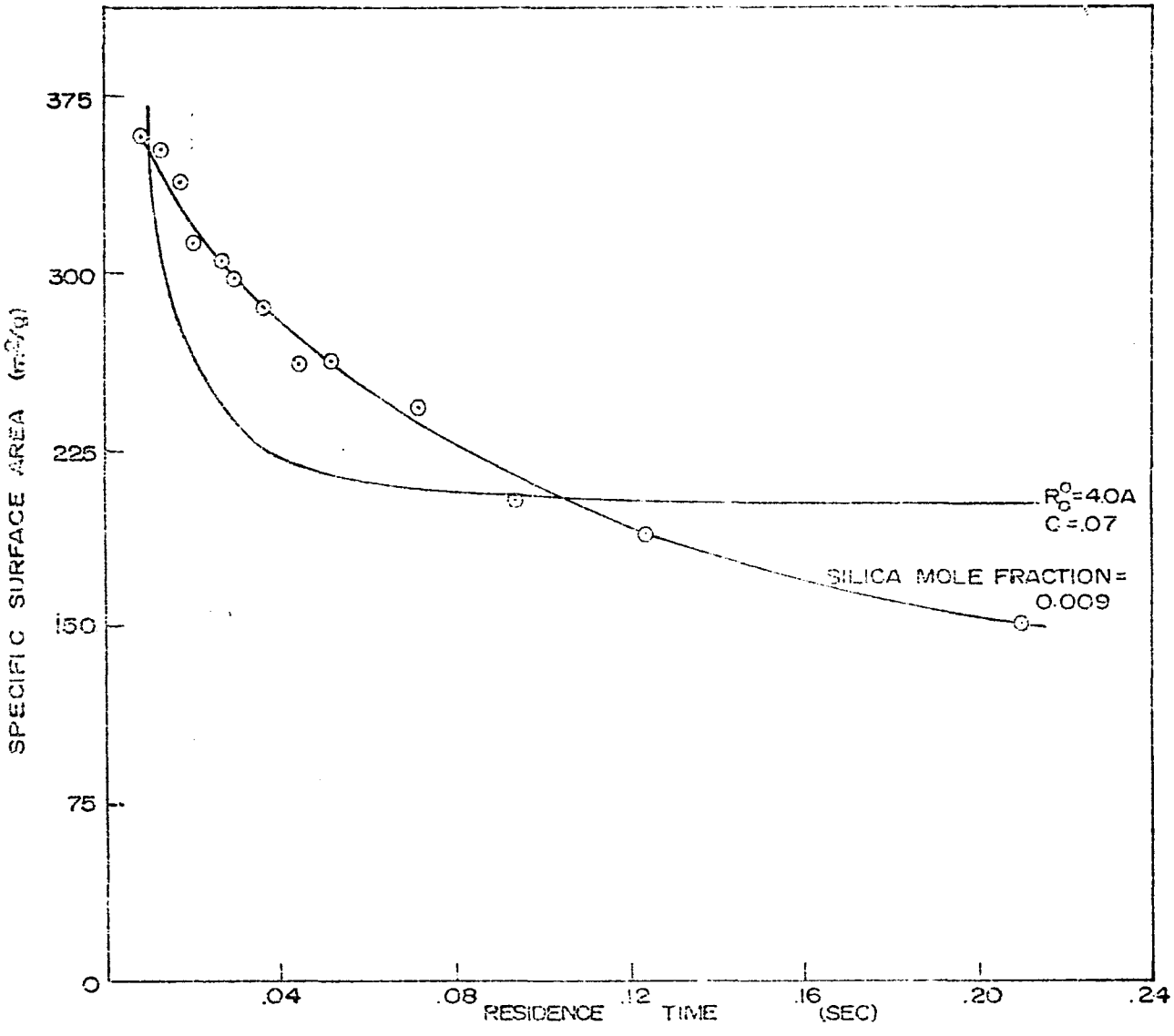

FIGURE 18. PLOT OF SA VERSUS RESIDENCE TIME

a. The use of incorrect collision cross section for aggregates.

b. The use of the numerical value of the bulkiness factor determined for carbon blacks. In the absence of any morphological parameter values for silica, its use seems valid, Cochrane (1974).

c. Knudsen number values calculated for some of the typical silica aggregates using the collision cross section expression (eq. 9) ranged from 1 to 20. This indicates that even though majority of the growth occurs in the free molecule aerosol region, some growth occurs in the transition region as well.

Experimental data were reproducible with regard to surface area results within plus or minus five percent. Of the last three reasons, item three is thought to be the most important. Andreas (1965) points out that serious theoretical questions arise if bulk values for surface tension (σ) and viscosity (μ) are considered for nuclei. However, no data were found in the literature for small particles.

Since experimental surface area data are reliable, hypothetical (σ/μ) values have been calculated by force fitting eq. 24 to these data.

$$\frac{d(SA)}{dt} = -\frac{0.22}{\rho R_o^2}\left(\frac{\sigma}{\mu}\right) \tag{24}$$

Figure 19 is a plot of these (σ/μ) values as a function of residence time. These results were then substituted into eq. 19 and numerically solved to obtain corrected values of N_P. These are shown in figure 20 along with experimental and theoretical curves from figure 16. The slope of the modified theoretical curve is in better agreement with experimental results than the curve based on bulk values of (σ/μ), but absolute values of N_P differ significantly except for the shorter

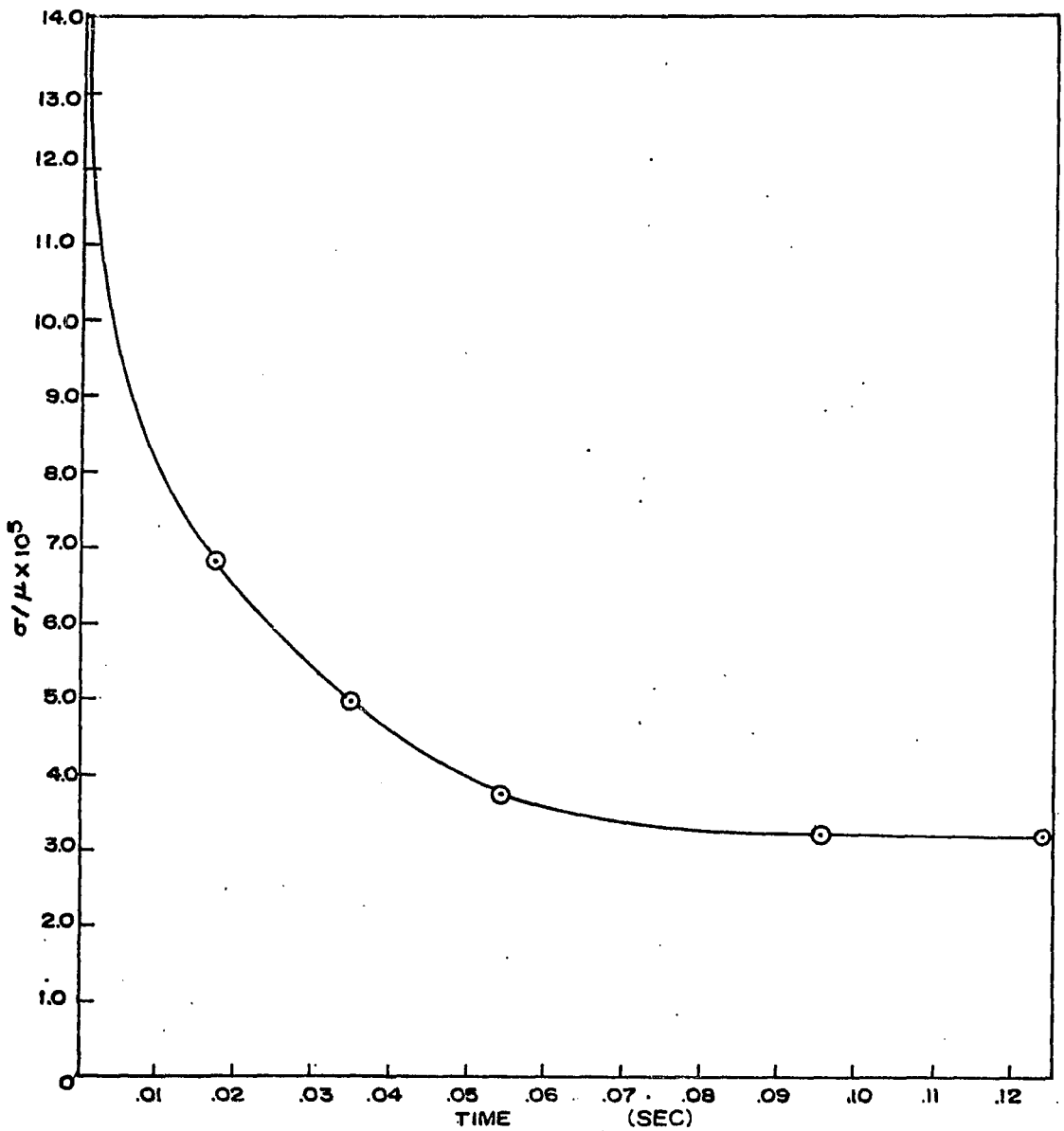

FIGURE 19. PLOT OF (σ/μ) VERSUS RESIDENCE TIME

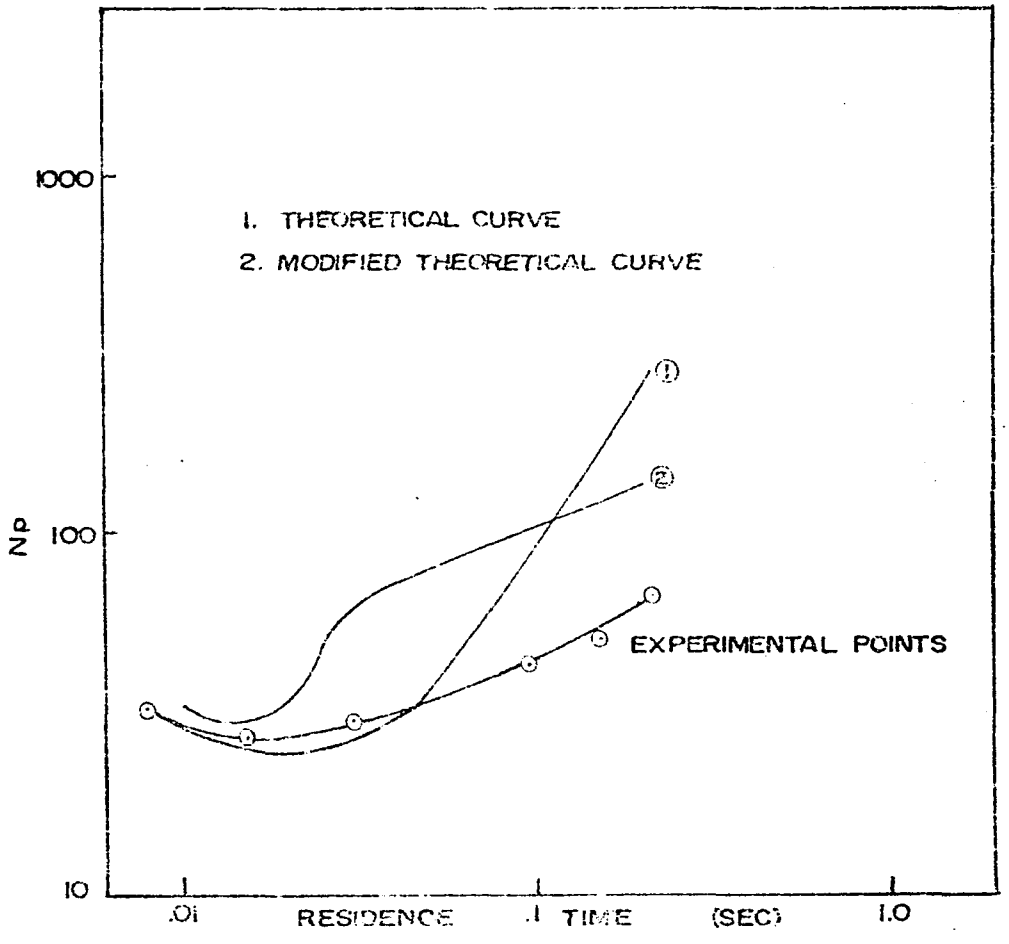

FIGURE 20. PLOT OF Np VS. RESIDENCE TIME USING THE REVISED (σ/μ) VALUES

residence times. Since the shorter residence time values apply to samples nearest the flame front, and since they are comparable to probe quench time (see Appendix B), they may be questioned. An alternate comparison may be made by fitting the theoretical and modified theoretical curves to an intermediate datum point. This has been done with the results shown in figure 21. The corresponding required values of R_o^o and c are 2A & .043 respectively. However, such a value of R_o^o cannot be justified from physical reasoning. One possible explanation may be that the sticking coefficient varies with residence time. It is not feasible at this point to justify further manipulations.

Conclusions:

The work reported in this investigation is the first detailed study of particle growth in oxide synthesis flames. From a theoretical standpoint, it is an improvement over the earlier theory of Brownian collision and coalescence. For example, based on the simplified model, aggregation was considered to be a transition process at the end of the growth period. In the improved model, aggregation is an integral part of the growth process. This is confirmed by electron micrographs which show aggregates present at all stages of the growth process.

Based on the refined model, a new relationship between particle concentration, particle size, and aggregate size has been developed. Since there are three arbitrary parameters in this theoretical expression, almost any set of experimental data can be accomodated, although the parameters required to fit the results are reasonable. Nevertheless, further work is necessary where systems of other oxides having different physical properties can be studied. Also, more

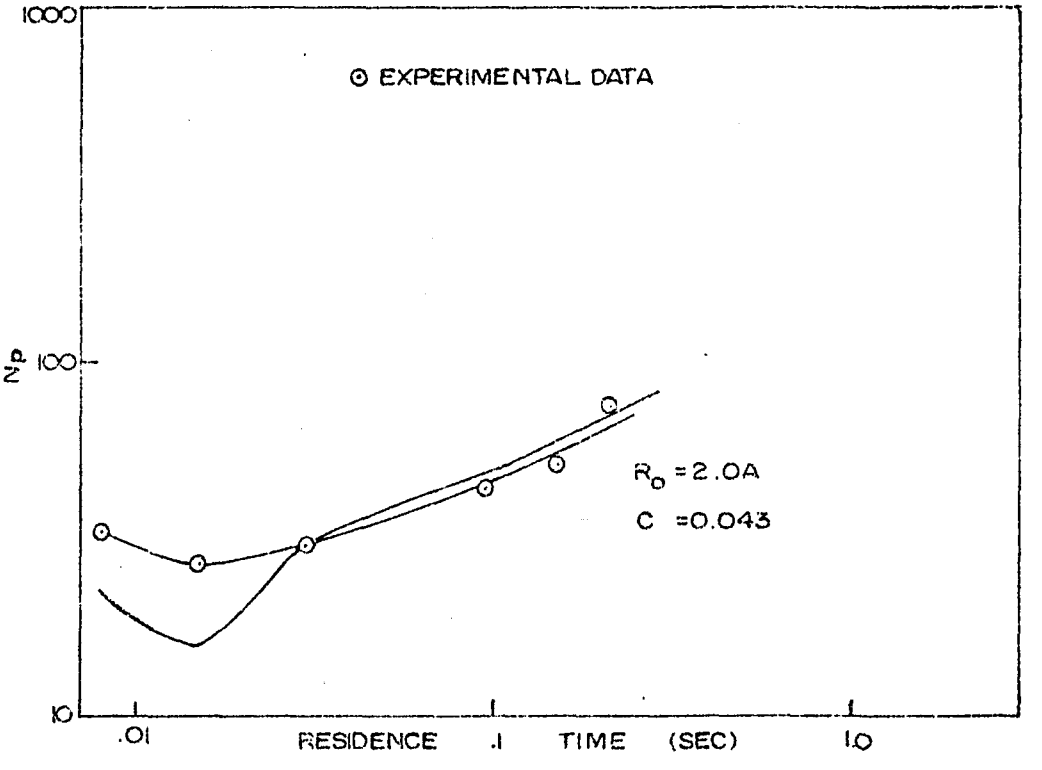

FIGURE 21. PLOT OF Np VS. TIME OBTAINED BY FITTING INTERMEDIATE DATUM POINTS

isothermal flames with broader residence time ranges would provide a better test of the theory. Also needed is an accurate means of evaluating N_P. Since the theory proposed here shows dependence of N_P on R_o^o, further work is necessary to look into the earlier growth regions where nucleation and surface reaction are predominant.

A better understanding of the growth phenomena as a whole will aid in the prediction of growth rates for commercial system such as fly-ash formation in boilers.

APPENDIX A

LABORATORY BURNER DESIGN CALCULATIONS

Basis: Assuming that the feed gases are entering at 220°F and 1 atmosphere pressure into the burner at a velocity of 1 ft/sec and assuming a maximum primary burner diameter of 1.5" the total gas flow rate through the burner can be calculated as follows:

$$\text{Total gas flow rate} = 1\ (\text{ft/sec}) \frac{\pi(\frac{1.5}{12})^2}{4}\ \text{ft}^2 \times 3600\ \frac{\text{sec}}{\text{hr}}$$

$$= 44.2\ \text{ft}^3/\text{hr} = 0.089\ \text{lb mole/hr}$$

The stoichiometric combustion reaction can be written as follows:

$$SiCl_4 + \tfrac{1}{2}C_3H_8 + \tfrac{5}{2}O_2 \rightarrow SiO_2 + 4HCl + \tfrac{3}{2}CO_2 \qquad (A1)$$

Using 1000% theoretical hydrogen, the above equation can be rewritten as

$$SiCl_4 + 5C_3H_8 + 25O_2 \rightarrow SiO_2 + 4HCl + 15\ CO_2 + 18H_2O \qquad (A2)$$

Using 400% theoretical oxygen, we can determine the flow rates of each of the components.

	Moles	Basis: 0.089 lb mole/hr		
$SiCl_4$	1.0	.00084	0.143 lb/hr	0.71 cc/min
Oxygen	100.0	.084	31.3 SCFH	0.53 SCFM
Propane	5.0	.0042	1.59 SCFH	0.026 SCFM
	106.0	.08904		

Having calculated the flow rates through the burner, we can determine the settings on the flowmeters corresponding to the above flowrates. In order to determine the velocity through the burner exit, plots are made between gas velocity and flowmeter settings. From these we can determine the actual cold gas velocity corresponding to actual settings used on the flowmeter in getting a flat flame. The actual temperature of the feed gases can be read from the pyrometer located on the instrument panel and necessary corrections can be made to the calculated design gas flow rate.

In addition to the main gas stream, there are two additional streams used in the laboratory burner. Through an annular opening of .005 inches, a hydrogen stream is passed which serves as a mantle flame as well as in anchoring the main flame to the burner tip. Through the annular space between the burner and the enclosed pyrex tube, air is passed at the same velocity as the combustion products which serves as an air curtain. The main purpose of the air curtain is to minimize mixing as well as to protect the pyrex tube from extreme heat exposure.

APPENDIX B

DETAILS OF PROBE DESIGN AND CONSTRUCTION

Probe sampling is straightforward, involving withdrawal, quenching and analysis. For flame applications, many problems have been solved in the use of probes for sampling. The recommended procedure involves use of a very fine microprobe usually made of quartz and the use of electron microscope, mass spectrometer or other analytical techniques for analysis. For the design and construction of probes for flame studies, Fristrom and Westenberg (1965) give an excellent review, and their technique has been successfully employed by many previous investigators.

The main problems in using quartz probes in the sampling technique are two fold. First of all, the tip of the probe becomes plugged soon after it was inserted into the flame, and secondly, there was not sufficient momentum to carry particles to the collection point, once they passed through the tip. Silica particles also tend to clog the quartz probe tip probably due to sintering and thermophoresis mechanisms.

To solve the above problems, it became necessary to design and construct a probe which would not be easily clogged at the tip or in the conveying line. This problem has been overcome successfully by developing a nitrogen quenched bend-free probe with a thin walled entry orifice. Dilution of the combustible products with dry nitrogen at the point of sampling not only helps carry the particles through the probe, but also helps prevent clogging of the probe tip. Nitrogen was passed through the annulus between two concentric tubes, the outer

tube having an orifice of diameter 0.020 inches. The inner tube (3/32" OD) was connected to the vacuum pump through the filter holder, where the particles were deposited. For flow through an orifice Fristrom and Westenberg (1965) give the following relation.

$$\dot{m} = CA'P \left\{ \frac{\gamma M}{R'T} \left(\frac{2}{\gamma+1} \right)^{\frac{\gamma+1}{\gamma-1}} \right\}^{1/2} \qquad \text{(B1)}$$

where C = 0.5 for small orifices

$\dot{m}$ = flow through orifice gm/sec

A'= orifice throat area sq.cm.

P = upstream pressure dynes/cm^2

γ = specific heat ratio

M = molecular weight

T = upstream temperature ^oK

R'= gas constant

Area of cross section of the orifice = 2.02 x $10^{-3} cm^2$.

Substituting M = 28.0, γ = 1.4, R' = 8.31 x 10^7 erg/mole^oK, P = 14.7 x 68947.6 dynes/sq.cm and T = 1975.0^oK into equation (B1) yields

$$\dot{m} = 0.53 \text{ gm/min} \qquad \text{(B2)}$$

Nitrogen flow rate = 375 cc/min at 25 psig

$$\dot{m} \quad \text{(for nitrogen)} = 0.47 \text{ gm/min} \qquad \text{(B3)}$$

Total flow of quench nitrogen and other combustion products through the probe tip is then 1.0 gm/min which is equal to 46 x 10^{-5} cuft/sec. The next step in the probe design is to check the absolute pressure at the orifice tip which should be at least half the operating pressure of the burner for creating sonic conditions at the tip. The increase to sonic velocity of the particles at the tip quenches further

reaction and growth of particles by the conversion of thermal energy to kinetic energy. The critical pressure ratio is given by

$$\frac{P_1}{P_2} = 0.547 \qquad \text{(B4)}$$

Since the burner is operating at atmospheric pressure the pressure at the throat must be less than or equal to 8.05 lb/inch^2. In order to check the actual pressure at the tip of the probe, let us calculate the value of the critical pressure.

Total flow rate through the probe tip = 0.0167 gm/sec.

Area of inside probe tube = 2.67 x 10 $^{-5}$sq.ft.

Hence Reynolds number is = 104

Since

$$\frac{-dP}{dz} = \frac{64}{N_{Re}} \frac{1}{D} \frac{PV^2}{2g_c} = 6.75 \text{psf/ft} \qquad \text{(B5)}$$

For dz = 2 ft, dP = 0.094 psi. Since the downstream end of the probe is connected to a vacuum pump operating at 20 mm Hg the pressure at the tip of the probe is well within sonic velocity conditions.

The opening of the probe is 0.02 inches and was chosen after considerable trial and error with various tip openings. In particle-laden streams, blockage of the sample hole has required very brief sampling periods or large holes. The blockage was influenced by probe temperature and internal deposition. The main criteria for the selection of 0.02 inches opening was to obtain sufficient sample quantities for evaluation without a severe loss of spacial resolution. Holes smaller than 0.02 inches did not remain open.

The weighed samples were compared against the theoretical values for a check on the material balance. The values agreed on the average within 10% and this could be attributed partly to the fact some of the samples inside the inner tube were not completely recoverable (see Table V).

Calculation of Quench Time: (Streeter 1971)

In this section calculations for evaluating quench time are presented. This will be a correction to the calculated residence times from velocity and temperature measurements.

Equation of Continuity

$$\dot{m} = \rho UA = \text{constant} \tag{B6}$$

The velocity U is given by

$$U = \bar{M} \sqrt{\frac{\gamma g_c RT}{M}} \tag{B7}$$

where $\bar{M}$ is the mach number, M is the molecular weight and γ is the ratio of specific heats.

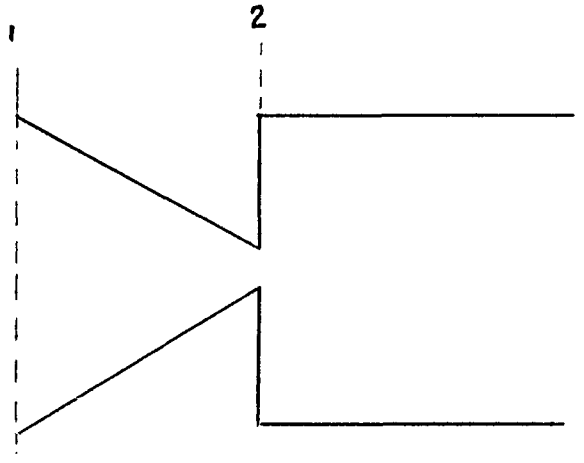

FIGURE B1

TABLE V

Material Balance Check on Collected Samples

Sample No.	Theoretical amount of sample (mg)	Actual amount of collected samples (mg)	% Difference
1	40.0	34.0	15.0
2	41.0	35.8	12.7
3	48.0	41.3	14.0
4	72.0	62.8	12.8

Sample Calculations:

From the equilibrium product composition.

20 moles of gas contain 0.142 moles of SiO_2

$(\frac{0.53}{28})\ \frac{\text{moles}}{\text{min}}$ of gas would contain = 8 mg/min of SiO_2

Assuming a coefficient value of C = 0.25, the amount collected in 10 minutes would equal 40.0 mgm.

Equation of Energy (See Figure B1)

$$\frac{T_2}{T_1} = \frac{1 + \frac{1}{2}(\gamma-1)\,\bar{M}_1^2}{1 + \frac{1}{2}(\gamma-1)\,\bar{M}_2^2} = 1.2 \qquad \text{(B8)}$$

Since $T_2 = 1975^{\circ}K$, $T_1 = 1646\ ^{\circ}K$

$$\rho = \frac{PM}{RT} = 0.9 \times 10^{-4}\ \text{lb/ft}^3$$

and

$$\frac{P_2}{P_1} = \left(\frac{T_2}{T_1}\right)^{\frac{\gamma}{\gamma-1}} = 1.89$$

Since the burner is operating as atmospheric pressure

$$P_1 = 0.53\ \text{atm (abs)}$$

U at the probe tip equals from eq (B7)

$$\frac{1.4 \times 32.2 \times 1546 \times 1.8 \times 1646}{60} = 1860.0\ \text{ft/sec}$$

Assuming that particles come into the influence of the probe at a distance of 5/64" (radius of the probe) and also considering that the area of cross section varies linearly between stations 1 and 2 an average velocity can be calculated. From this the quench time can be obtained

$$U_{ave} = 66.0\ \text{ft/sec}$$

hence quench time = .0001 secs.

APPENDIX C

DETAILS OF SAMPLE PREPARATION AND ANALYSIS

The samples collected at various heights above the flame front were analysed for quantitative and qualitative information. The obtained samples were calcined first to remove HCl from the surface and a measurement of the weight of the sample before and after calcination indicated a weight loss of 7 - 15%.

Measurement of Surface Area by Adsorptograph:

Surface area determination involves measuring the amount of gas adsorbed on a solid surface at a temperature close to the boiling point of the gas. Nitrogen is most widely used as the adsorbate. Ordinarily the B.E.T. equation is used in order to calculate the amount of adsorbate to form a monolayer and this amount when multiplied by proper factors for area covered per unit amount of nitrogen gives the surface area. The adsorptograph uses thermal conductivity measurements of adsorbate concentration in a continuous helium stream rather than pressure volume measurements using a calibrated glass vacuum apparatus. The thermal conductivity of a mixture of helium and nitrogen gas is monitored differentially by thermal conductivity cells, placed before and after the sample. Experimentally after a number of trial and error calculations, it has been determined that for the highest precision it is necessary to set up a strict empirical procedure for a set of samples.

The adsorptograph is very similar to a gas chromatograph, with the column packing as the sample. Details of the equipment are described by Atkins (1964). The procedure followed in the measurement of surface area is as follows. Initially weigh a certain amount of the

sample (approximately 10 - 15 mg depending where the peak occurs) using a vibratory spatula. The amount of the sample can be approximately known from a rough estimate of the specific surface area. From trial and error, it has been determined that it should be the value obtained by dividing the factor 5.2 by the surface area. The amount of sample should fill no more than the lower half of the adsorption cell. Initially outgas the sample by placing a tube furnace at 100°C around the adsorption cell. Then remove the tube furnace and place a Dewar flask of liquid nitrogen around the adsorption cell. When the recorder pen comes to the base line remove the Dewar of liquid nitrogen from around the adsorption cell and immediately replace the tube furnace. The desorption peak like the degassing peak will appear on the chart recorder and the area under the desorption peak is then determined for obtaining surface area.

The desorption peak should occur around 60 - 90 on the recorder chart for accuracy and reproducibility. If it falls below the indicated value, a larger amount of the sample is weighed and the procedure repeated and vice versa if the peak goes beyond 90.

Basis of calculation:

The Brunauer-Emmett-Teller known as the B.E.T. equation is given by

$$\frac{P}{V_{ads}(P_o-P)} = \frac{C-1}{V_m C}\frac{P}{P_o} + \frac{1}{V_m C} \qquad (C1)$$

This is the isotherm equation of the multimolecular theory for adsorption taking place on a free surface. It is a linear equation when $\frac{P}{V_{ads}(P_o-P)}$ is plotted against P/P_o where

V_{ads} = Total volume of adsorbed gas on the surface of the sample (cc)

V_m = Volume of adsorbed gas when the entire adsorbent is covered with a monomolecular layer (cc)

P = Partial pressure of adsorbate (mmHg)

P_o = Saturation pressure of the adsorbate on the sample at the temperature of the coolant (mmHg)

C = Constant expressing the net adsorption energy

The adsorptograph is mainly a single point instrument, which assumes an intercept of zero in the B.E.T. plot, which is seldom correct. However, when comparing various samples we are more interested in relative values rather than absolute values. For cab-o-sil the B.E.T. volumetric method agrees very well with single point determinations within 4 - 5%. Also B.E.T. method would require greater quantity of the sample as well as time than the adsorptograph method.

In order to eliminate possible sources of error, a comparator technique is used where the desorption peak of a known surface area carbon black is compared against the desorption peak of unknown silica samples.

$$\text{Sample surface are} = \Sigma_c \, \gamma'/\sigma' \qquad \text{(C2)}$$

σ' = Sample Integral/gm

γ' = Comparator Integral/gm

Σ_c = Comparator surface are (m^2/gm)

Preparation of sample for EM analysis:

The surface area measurements give us a comparison of the samples obtained at various heights from the flame front with regard to average particle size. To obtain further qualitative and quantitative

information about the samples, we have resorted to the use of electron microscopy. The electron microscopy by far is the most extensively used technique to study the "structure" of very fine particles. In order to prepare the grids for EM analysis, the procedure outlined by Medalia and Heckman (1969) has been adopted with some modification. Various methods of dispersion of the samples have been tried in order to obtain good electron micrographs.

The silica samples initially are dispersed in diluted collodion (Fisher Scientific Co. No. C 407) diluted 1:40 in ethyl acetate, by means of ultrasonic energy. To this mixture a drop of castor oil is added. Initially 3 mg of the samples are weighed into a vial to which 30 cc of the mixture of diluted collodion is added. The vial is then immersed into an ice bath and an ultrasonic probe is inserted and run with a power output of 75 w at 20kc/sec for 10 minutes. A glass slide 1 x 3" (Fisher Scientific Co) is then dipped into the dispersed solution, drained of excess liquid and stood up to air dry. After the slides are dried for about an hour in a dust free atmosphere the edges of the film are scored and it is floated off on water and picked up on a carbon substrate, 300 mesh electron microscope specimen grid. The grids are then air dried and then washed overnight in ethyl acetate to remove the collodion film. After letting it dry for about 20 minutes, the grids are ready to be seen under the electron microscope.

In order to avoid operator bias, micrographs are taken of 4 random grid openings (out of 530 visible in the electron microscope) to obtain representative coverage over the entire grid. Electron image plates (3-1/4" x 4") have been used and Kodak H.R.P. developer was used to develop the negative plates. A magnification of 30,500 was used on

the electron microscope (Phillips EM-200) which was further magnified on the enlarger, to get a final magnification of 100,000X. Kodak #2 paper was used to get the necessary contrast in the 8" x 10" prints.

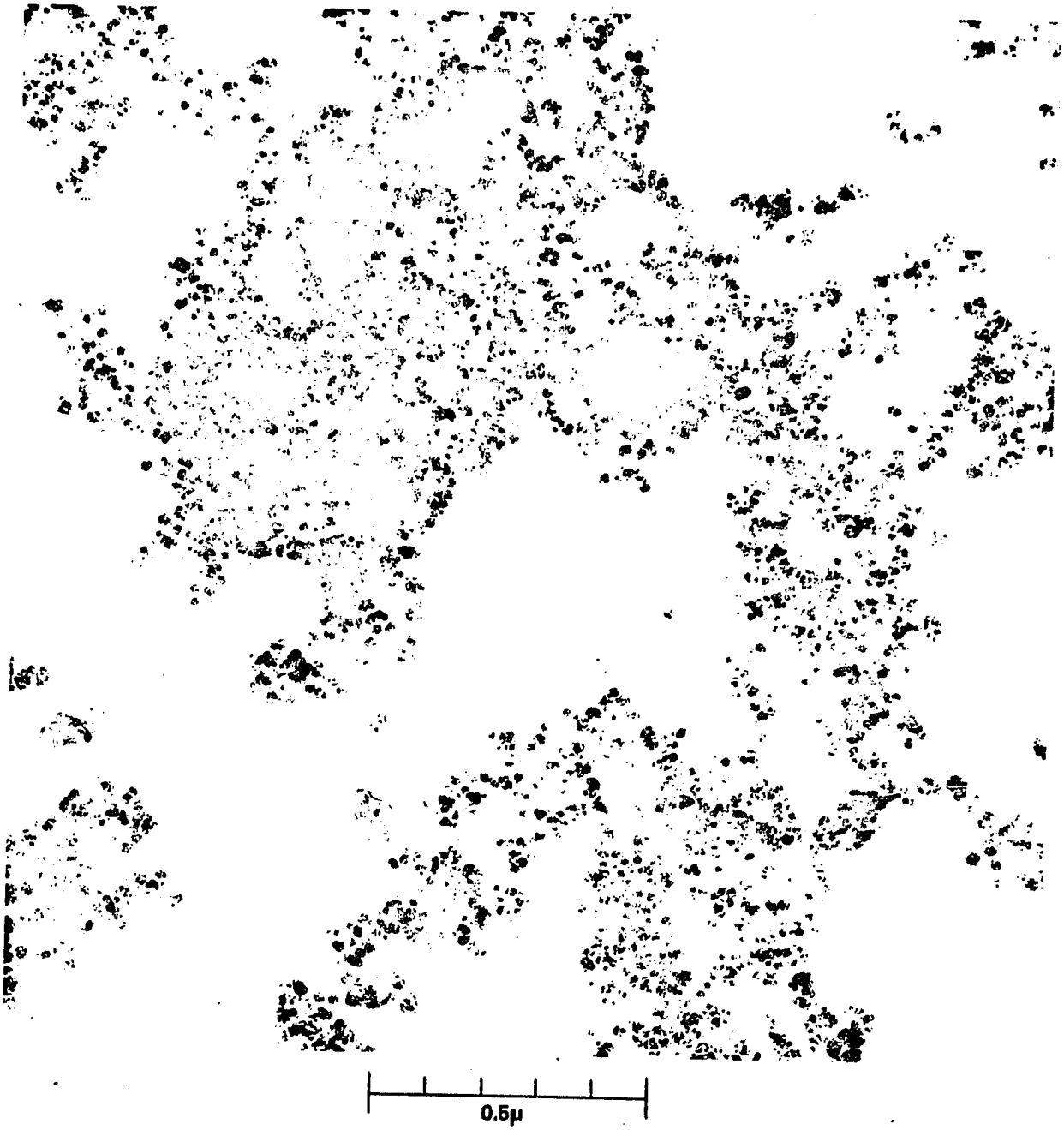

100,000 X
TRANSMISSION ELECTRON MICROGRAPH

SAMPLE COLLECTED DIRECTLY ON CARBON GRID
(NO DISPERSION OF THE SAMPLES WAS UNDERTAKEN)

APPENDIX D

COMPUTER PROGRAM FOR THE EVALUATION OF EQUILIBRIUM TEMPERATURES AND COMPOSITIONS OF COMPLEX CHEMICAL SYSTEMS

The theoretical calculations which yield equilibrium temperatures and compositions of complex chemical system such as our silica flame, are extremely lengthy and repetitious. Accordingly, the program used by Cruise (1964) for evaluating rocket propellant performance has been considerably modified to be run on IBM 360/50 facilities of the Computation Center, University of New Hampshire.

The program operates under the following assumptions:

1. Thermodynamic Model: The program assumes adiabatic combustion with no work (other than PV work) done by the gases and negligible kinetic and potential energies. The neglecting of the kinetic and potential energies, is valid for almost all flame system and under the above assumption the feed and product enthalpies are equal.

2. Ideal Gases: Ideal gas law is assumed, whereby enthalpy is not dependent upon pressure. Also gas fugacities equal the partial pressures which in turn can be written as a product of mole fraction and total pressure. This assumption in unquestionably valid at the temperatures and pressures that exist in most flame systems.

3. Kinetic Model: The program lists output, which are final equilibrium conditions only. These conditions are undoubtedly approached in our silica synthesis flames.

4. Condensed Species: If two or more condensed species are present they are treated as immiscible. Though this is valid for silica flames, it is not necessarily true for fly ash problems.

5. Species List: The program also uses a tape which contains the product species and thermodynamic data. The data set name assigned to this library tape is SERGIO. Before using the program, it is essential that all species which may be important in a given system are included among the species list. Otherwise the results will be in error. If a given product species is not included in the library tape, it can be easily added to it.

Method of Providing Data and Results:

The first column of the first data card contain option switches. The details of the available options can be found in the information manual for the theoretical propellent evaluation program, Cruise (1964). Column 20 is used to specify the type of the system being run, as S = Solid, L = Liquid, G = Gas and H = Hybrid. The above specification is for bookkeeping purposes only. Column 21 through 24 contain the name of the person running the program. Ending in column 28 is the number of (not more than 10) flame ingredients. Ending in column 38 is the number of runs to be made on the system of ingredients.

Typical results of cab-o-sil flame are given in this appendix. We are mainly interested in determining theoretical flame temperature. Other application of these results can be to determine the effect of species concentrations and theoretical flame temperature as a function of feed parameters. This could be useful in any commercial production of silica.

PANI

INGREDIENTS	H	C	N	O	SI	CL							WEIGHT	CAL./G.	DENSITY
PROPANE	C.CC8	0.003	0.0	0.0	C.0	0.0	0.0	0.0	0.0	0.0	0.0	0.0	27.200	-564.	0.0
OXYGEN	0.0	0.0	0.0	0.002	0.0	0.0	0.0	0.0	0.0	0.0	0.0	0.0	435.800	0.	0.0
SILICON TETRACHLORIDE	0.0	0.0	0.0	0.0	C.001	0.004	0.0	0.0	0.0	0.0	0.0	0.0	24.060	-919.	0.0
NITROGEN	C.C	0.0	0.002	0.0	C.0	0.0	0.0	0.0	0.0	0.0	0.0	0.0	135.000	0.	0.0

GRAM ATOM AMOUNTS FOR PROPELLANT WEIGHT OF 622.060 **********

(H)	(C)	(N)	(O)	(SI)	(CL)	(
4.934574	1.650465	9.637351	27.237473	0.141558	0.566391	

CHAMBER RESULTS	TEMP.(K) 1975.	TEMP.(F) 3096.	PRESS.(ATM) 1.00	PRESS.(PSI) 14.7000	ENTHALPY -37.45	ENTROPY 1331.70	FCGMASS 1.2524	MOLS GAS 19.992	RT/V 0.0500

C	0.0000	(2.25E-21)	CCCL2	0.0000	(8.01E-12)	CO	0.0027	(2.70E-03)	CO2	1.8478	(1.85E CC)
CL	0.0825	(8.25E-02)	HCL	0.4811	(4.81E-01)	HOCL	0.0004	(4.41E-04)	CCL	0.0009	(9.06E-04)
SICL	0.0000	(2.78E-16)	CL2	0.0007	(7.43E-04)	SICL2	0.0000	(1.46E-12)	SIHCL3	0.0000	(3.94E-16)
SICL4	0.0000	(2.78E-12)	H	0.0002	(1.64E-04)	NH	0.0000	(1.12E-09)	HO	0.0492	(4.92E-02)
SIH	0.0000	(2.61E-23)	H2	0.0007	(7.25E-04)	H2O	2.2011	(2.20E CO)	NH3	0.0000	(3.76E-11)
N	0.0000	(6.08E-05)	NO	0.1315	(1.31E-01)	NO2	0.0003	(3.45E-04)	N2	4.7528	(4.75E CC)
N2O	0.0000	(3.66E-06)	O	0.0079	(7.90E-03)	SIO	0.0000	(3.53E-07)	C2	10.4321	(1.04E 01)
SIO2	0.0000	(8.53E-06)	SI	0.0000	(3.69E-16)	NHO	0.0000	(3.19E-07)	E-	0.0000	(8.84E-14)
HCL&	0.0000	(2.15E-16)	H3O&	0.0000	(2.03E-11)	O-	0.0000	(1.62E-15)	O2&	0.0000	(1.41E-14)
O2-	0.0000	(2.49E-14)	SI&	0.0000	(1.94E-20)	CL-	0.0000	(1.04E-09)	NC&	0.0000	(1.02E-09)
HO-	0.0000	(1.70E-14)	SIO2*	0.1416	(1.42E-01)	SIC*	0.0	(0.0)	SIC$	0.0	(0.0)
C$	0.0	(0.0)	SI3N4$	0.0	(0.0)	SIO2$	0.0	(0.0)			

APPENDIX E

COMMENTS AND RECOMMENDATIONS ON PARTICLE SIZE MEASUREMENT IN THE ELECTRON MICROSCOPE

(Communicated by F.A. Heckman, Cabot Corporation, Billerica, Mass.)

During the last several years most carbon black electron microscopists have almost completely abandoned hope for making accurate and precise particle size measurements from electron micrographs, using current technology. This state of affairs is due to several considerations both theoretical and practical.

First of all, one must realize that modern furnace blacks consist of aggregates (the smallest dispersable units of carbon black). Aggregates are in turn composed of "particles" which are thoroughly and extensively fused together. This high degree of fusion makes particle discernment and identification a very arbitrary and subjective process. Thus, when one has a material which is <u>not</u> composed of descrete spheres it is not possible to describe its morphology accurately in terms of spherical parameters such as particle diameter.

Second, the number of measurements (1,000 to 2,500) which can be made in a reasonable time is inadequate to represent the sample in a statistically reliable manner. This fact has been demonstrated repeatedly in the past by attempts to get good reproducibility on coded replicate samples.

Third, our efforts to increase objectivity by photographing pre-selected random fields and by using statistically reliable methods for sampling the fields photographed have met with only limited success.

All of the above considerations combine to make particle size study by current electron microscopy methods an expensive exercise in futility. Thus we recommend that electron microscope determination of carbon black particle size be discontinued and that average particle size be computed from the specific surface area of the black. Specific surface areas may be measured by Nitrogen adsorption techniques such as the BET and "t" methods, or by the recently introduced CTAB method. One may compute the surface average particle diameter DA in millimicrons ($m\mu$) by using the following equation

$$DA = \frac{6000}{\rho SA} \qquad (E1)$$

where 6000 is a constant and ρ is the specific gravity (for silica ρ equals 2.2) and SA is the surface area expressed on square meter per gm m^2/g.

It should be noted that values computed by this method average about 20% higher than the corresponding values from electron microscopy. Also, it is very important to note the <u>number</u> average diameter or the Arithmetic mean diameter DN (which most people use for the "EM particle size" value) is about 25% lower than DA for conventional tread blacks and about 10% lower for new technology tread blacks.

Finally, we would like to make it clear that certain other carbon black morphology parameters such as aggregate size and shape (and their distribution) can be determined with much greater accuracy and precision than the elusive "particle size". Several workers in carbon black research have used fully automated or semi-automated techniques with reasonable success to determine aggregate parameters. Also, it should be emphasized that much useful information is obtainable,

simply by making qualitative comparisons of electron micrographs. In this way, one can roughly evaluate such interesting characteristics as uniformity, dispersibility and gross differences (or similarities) in "particle" size and aggregate size.

LITERATURE CITED

Andreas, R. P. (1965), Homogeneous Nucleation from the vapor phase, Ind. Eng. Chem. 57(10), 25.

Atkins, J. H. (1964), Rapid and precise method for determining surface areas, Analytical Chemistry 36 (3), 579.

Ball, R. T. and Howard, J. B. (1971), Electric charge of carbon particles in flames, Thirteenth symposium (International) on combustion, P. 353, The Combustion Institute.

Bonne, U., Homann, K. H., and Wagner, G. Gg (1965), Carbon formation in premixed flames, Tenth symposium (International) on combustion, P. 503, The Combustion Institute.

Boonstra, B. B., Dannenberg, E. M. and F. A. Heckman (1974), The effect of carbon black structure breakdown on rubber properties. Paper to Fourth European conference on Plastics and Rubbers, Paris.

Cochrane, H. (1974), Cabot Corporation, Billerica, Mass., Personal Communication.

Courtney, W. G. (1967), Condensation during hetrogeneous combustion. Eleventh symposium (International) on combustion, P. 237. The Combustion Institute.

Cruise, D. R. (1964), Information manual for the theoretical propellent evaluation programs, USNOTS.

Fenimore, C. P. and G. W. Jones (1969), Coagulation of Soot to smoke in hydrocarbon flames, Combustion and Flame, 13, 303.

Frenkel, J. (1945), Viscous flow of crystalline bodies under the action of surface tension, J. of Physics 9 (5), 385.

Friedlander, S. K. (1973), Small particles in air pose a big control problem,

Environmental Science and Technology, 7 (13), 1115.

Fristrom, R. M. and Westernberg, A. A. (1965), Flame structure, P. 180, McGraw-Hill.

Goodrich, F., "Study of Particle morphology for surface deposition," Seminar presented at Cabot Corporation, Billerica, Mass, (1967) (communicated by Professor Gail D. Ulrich).

Hardesty, D. R. and Weinberg, F. J. (1973), Electrical control of particulate pollutants from flames, Fourteenth Symposium, (International) on Combustion, The Combustion Institute, P

Heckman, F. A. (1974), Cabot Corporation, Billerica, Mass., Personal Communication.

Hermsen, R. W. and Dunlap, R. (1969), Nucleation and growth of oxide particles in metal vapour flames, Combustion and Flame 13, 253.

Hidy, G. M. (1965), On the theory of the coagulation of noninteracting particles in Brownian motion, J. Colloid, Sci., 20, 123.

Homann, K. H. (1967), Carbon formation in pre-mixed flames, Combustion and Flame 11, 265.

Homann, K. H. (1968), Soot formation in pre-mixed hydrocarbon flames, Angew, Chem. Internat. Edit. 7(6), 414.

Howard, J. B., Wersborg, B. L. and Williams, G. C. (1973), Coagulation of carbon particles in premixed flames, Faraday symposia of the chemical society 7, 109.

Howard, J. B. (1969), On the mechanism of carbon formation in flames, Twelfth symposium (International) on combustion, The Combustion Institute, P. 877.

Kingery, W. D. (1960), Introduction to ceramics, P. 574, John Wiley & Sons.

Mayo, P. J. and Weinberg, F. J. (1970), On the size, charge and number rate of formation of carbon particles in flames subjected to electric fields, Proc. Roy. Soc. Lond. Series A, 319, 351.

Medalia, A. I. (1967), Morphology of Aggregates: Calculation shape factors; Application to computer simulated random flocs, J. of Colloid and Interface Sc. 24, 393.

Medalia, A. I. and Heckman, F. A. (1969), Morphology of Aggregates: Size and shape factors of carbon black aggregates from electron microscopy, carbon, 7, 567.

Milnes, B. (1974), M.S. Thesis to be submitted to the Department of Chemical Engineering, University of New Hampshire, Durham.

Place, E. R. and Weinberg, F. J. (1967), The nucleation of flame carbon by ions and the effect of electric fields, Eleventh Symposium (International) on Combustion, The Combustion Institute, P. 245.

Smoluchowski, M. (1917), Versuch Einer Mathematischen Theorie der Koagulationskinetik Kolloider Losungen, 2, Phys. Chem. 92, 129.

Streeter, V. L. (1971), Fluid Mechanics P. 325, McGraw Hill.

Sutherland, D. N. and Goodarz-nia, I. (1971), Floc simulation: the effect of collision sequence, Chemical Engineering Science, 26, 2071.

Ulrich, G. D. (1971), Particle Formation in oxide synthesis flames, Comb. Sc. and Tech. 4, 47.

Ulrich, G. D. (1969), "Comments," Twelfth Symposium (International) on Combustion, P. 884, The Combustion Institute.

Wersborg, B. L., Howard, J. B. and Williams, G.C. (1973), Physical mechanism in carbon formation in flames, Fourteenth symposium (International) on combustion, The Combustion Institute, P. 929.

NOMENCLATURE

A	Avagadro's number (6.023×10^{23})
$\overline{A}$	Projected area of a floc (cm^2)
A'	Throat area (cm^2)
B	Bulkiness factor
c	Sticking coefficient (ratio of successful to actual collisions)
C_o	Total concentration of condensible species (molecules cm^{-3})
h	Heat transfer coefficient Btu/hr $ft^{2o}F$
K	Coagulation rate constant
Kn	Knudsen number
k	Boltzmann's constant (1.38×10^{-16} erg $molecule^{-1}$ deg^{-1})
L	Collision frequency (sec^{-1})
m	Aggregate mass (g)
M	Molecular weight (g $mole^{-1}$)
$\overline{M}$	Mach number
N	Aggregate concentration (number cm^{-3})
N_i	Concentration of particle size i (number cm^{-3})
N_{Re}	Reynolds number
N_o	Initial particle concentration (number cm^{-3})
N_p	Number of particles per aggregate
R	Aggregate collision cross section (cm)
R'	Gas constant
R_o	Primary particle radius (cm)
R_o^o	Initial primary particle radius (cm)
SA	Specific surface area (m^2/g)
t	Residence time (sec)

t_f	Time for complete coalescence (sec)
T	Absolute temperature (^{o}K)
U	Velocity
y	Correction factor
ρ	Particle density (gcm^{-3})
σ	Surface tension (dyne cm^{-1})
μ	Viscosity (poise)
γ	Specific heat ratio